ORNL
MASTER COPY
APR 3 - 1995

ORNL/M-4079

ornl

OAK RIDGE
NATIONAL
LABORATORY

MARTIN MARIETTA

DEVELOPMENT OF OPTIMUM POWDERS FOR POWDER EVACUATED PANEL INSULATION

K. E. Wilkes
Oak Ridge National Laboratory

P. W. Lucas
PPG Industries

MANAGED BY
MARTIN MARIETTA ENERGY SYSTEMS, INC.
FOR THE UNITED STATES
DEPARTMENT OF ENERGY

This report was prepared as an account of work sponsored by an agency of the United States Government. Neither the United States Government nor any agency thereof, nor any of their employees, makes any warranty, express or implied, or assumes any legal liability or responsibility for the accuracy, completeness, or usefulness of any information, apparatus, product, or process disclosed, or represents that its use would not infringe privately owned rights. Reference herein to any specific commercial product, process, or service by trade name, trademark, manufacturer, or otherwise, does not necessarily constitute or imply its endorsement, recommendation, or favoring by the United States Government or any agency thereof. The views and opinions of authors expressed herein do not necessarily state or reflect those of the United States Government or any agency thereof.

ORNL/M-4079

Metals and Ceramics Division

DEVELOPMENT OF OPTIMUM POWDERS FOR POWDER EVACUATED PANEL INSULATION

K. E. Wilkes

P. W. Lucas
PPG Industries

Date Published - February 1995

Prepared for the
U. S. Department of Energy
Office of Buildings Energy Research

and

PPG Industries, Inc.

Prepared by
OAK RIDGE NATIONAL LABORATORY
Oak Ridge, Tennessee 37831
managed by
MARTIN MARIETTA ENERGY SYSTEMS, INC.
for the
U.S. DEPARTMENT OF ENERGY
under contract DE-AC05-84OR21400

TABLE OF CONTENTS

LIST OF FIGURES v

LIST OF TABLES vii

ABSTRACT 1

1. OBJECTIVES OF CRADA 2

2. MATERIALS SYNTHESIS AND CHARACTERIZATION 4
   - 2.1 Synthesis of Silica Powders 4
   - 2.2 Characterization of Powders 4
   - 2.3 Materials Tested 6

3. ORNL EXPERIMENTAL METHODS 11
   - 3.1 Thermal Test Methods 11
   - 3.2 Preparation of Thermal Test Specimens 15

4. THERMAL TEST RESULTS 17
   - 4.1 Initial Powder Evacuated Panels 17
   - 4.2 Powders Tested at Tapped Density 17
   - 4.3 Variable Pressure Powder Evacuated Panels 43

5. CORRELATION OF HEAT CONDUCTION MECHANISMS WITH MORPHOLOGY 56
   - 5.1 Heat Conduction Mechanisms 56
   - 5.2 Correlation of Powder Characteristics with Thermal Conductivity 66

6. COSTS OF POWDERS 74

7. INVENTIONS 74

8. POSSIBLE COMMERCIAL APPLICATIONS 74

9. CONCLUSIONS AND POSSIBLE FUTURE COLLABORATIONS 74

10. REFERENCES 76

[redacted]

LIST OF FIGURES

1. Schematic of Heat Flow Meter Apparatus 12
2. Schematic of Radial Heat Flow Apparatus 14
3. Test Results for First Series of Powder Evacuated Panels 19
4. Effect of Density on Thermal Resistance of First Series of Powder Evacuated Panels . 20
5. Thermal Resistivity of Commercial Powders at Tapped Density 36
6. Thermal Resistivity of PPG Series 300 and 400 Powders at Tapped Density 37
7. Thermal Resistivity of PPG Series Y Powders at Tapped Density 38
8. Thermal Resistivity of Microcel Powders at Tapped Density 39
9. Thermal Resistivity of ORNL Powder at Tapped Density 40
10. Thermal Resistivity of Fly Ash at Tapped Density 41
11. Thermal Resistivity of Variable Pressure Powder Evacuated Panels 48
12. Normalized Thermal Resistivity of Variable Pressure Powder Evacuated Panels ... 49
13. Thermal Resistivity of BXS-363 PEPs and Powder 50
14. Thermal Resistivity of BXS-424 PEP and Powder 52
15. Thermal Resistivity of BXS-426 PEP and Powder 53
16. Thermal Resistivity of FK500LS PEP and Powder 54
17. Thermal Resistivity of Sipernat 22 LS PEP and Powder 55
18. Two Methods to Derive Effective Surface Spacing from Thermal Conductivity versus Pressure Curve (data are for BXS-427 powder) 60
19. Optical Constants for Silica Glass 61
20. Rayleigh Absorption Efficiency for Silica Glass 62
21. Normalized Spectral Contribution to Thermal Conductivity with and without Powder at 0.1 g/cm^3 65
22. Comparison of Two Ways of Estimating the Effective Surface Spacing 68
23. Correlation between Effective Particle Spacing and Particle Diameter 70
24. Comparison of Low Pressure Powder Thermal Conductivity with Results of Electromagnetic Theory 72
25. Effect of Density on Thermal Conductivity of Variable Pressure Powder Evacuated Panels 73

[redacted]

[redacted]

LIST OF TABLES

1. Characteristics of First Series of Powders 8
2. Characteristics of Second Series of Powders 8
3. Characteristics of Third Series of Powders 9
4. Characteristics of Fourth Series of Powders 9
5. Test Results on First Series of Evacuated Panels 18
6. Results of Radial Heat Flow Apparatus Tests on PPG Powders at Tapped Density ... 22
7. Results of Radial Heat Flow Apparatus Tests on Degussa Powders at Tapped Density 30
8. Results of Radial Heat Flow Apparatus Tests on Microcel Powders at Tapped Density 31
9. Results of Radial Heat Flow Apparatus Tests on ORNL Powder at Tapped Density .. 33
10. Results of Radial Heat Flow Apparatus Tests on Fly Ash at Tapped Density 34
11. Results of Heat Flow Meter Apparatus Measurements of Variable Pressure PEPs made with PPG Powders 44
12. Results of Heat Flow Meter Apparatus Measurements of Variable Pressure PEPs made with Degussa Powders 47
13. Estimates of Effective Interparticle Spacing for Powders at Tapped Density 67
14. Correlations of Graphically Determined Effective Surface Spacing with Specimen Characteristics 69

[redacted]

DEVELOPMENT OF OPTIMUM POWDERS FOR POWDER EVACUATED PANEL INSULATION*

K. E. Wilkes and P. W. Lucas**

ABSTRACT

A cooperative research and development agreement (CRADA) was signed by PPG and Martin Marietta Energy Systems, Inc. in August 1992. The purpose of the CRADA was to determine the relationship between the morphology of silica particles and the thermal conduction mechanisms operative in Powder-filled Evacuated Panel (PEP) insulation, and to optimize the cost versus thermal performance of the silica powders for PEPs. The CRADA was identified as ORNL 91-0071. Specifically, several silica based powders were synthesized and characterized by PPG and sent to ORNL for thermal resistivity (R) measurements and analysis.

One of the most promising applications of PEPs is in home refrigerators/freezers where estimates predict that about 0.6 quads (1% of the energy used in the U.S.) could be saved. Their use would also reduce the use of environmentally unacceptable insulation. This CRADA was performed over a period of 29 months. DOE's contribution to the project was approximately $190,000 and PPG's contribution was approximately $180,000.

---

*Research sponsored by the Office of Buildings Energy Research, U.S. Department of Energy, managed by Martin Marietta Energy Systems, Inc., under contract DE-AC05-OR21400, and by PPG Industries, Inc., as CRADA ORNL 91-0071.

**K. E. Wilkes, Metals & Ceramics Division, Oak Ridge National Laboratory; P. W. Lucas, PPG Industries, Inc.

[redacted]

1. OBJECTIVES OF CRADA

The purpose of this cooperative effort was to determine the relationship between the morphology of silica particles and the thermal conduction mechanisms operative in Powder-filled Evacuated Panel (PEP) insulation and to optimize the cost versus thermal performance of the silica powders for PEPs. Specifically, a series of silica-based powders were characterized by PPG Industries, Inc. and submitted to ORNL for determination of the thermal resistivity and correlation of the thermal conduction mechanisms with morphology. Based on these results, additional silica-based powders were characterized and submitted by PPG and tested by ORNL to further quantify the morphology/conduction relationship. After several iterations, the relationships among morphology, thermal performance, and cost of the silica-based powders were determined.

The objectives of the CRADA were met as shown in the following discussion. A large number of powders were characterized by PPG and were measured by ORNL. ORNL measurements included experiments on powders at tapped density and on powders formed into PEPs. In addition to experimental powders developed by PPG, several other powders were characterized and measured for thermal performance. These included several commercially available powders, a powder developed at ORNL, and powders based on fly ash. For fine powders at tapped density, the thermal performance at low pressures correlated most closely with the bulk density. As the density was increased, the thermal conductivity tended to decrease. This indicates that radiation is a large contributor to the thermal conductivity at low pressures. It was found that the thermal performance of relatively coarse powders could be improved significantly at intermediate pressures by jet-milling the powders to reduce the particles to the size of a few

[redacted]

microns. This indicates that the particle size has a strong influence on gaseous conduction by limiting the mean free path of the air molecules. PEP panels made from several PPG powders had similar thermal performance and little correlation between thermal conduction and particle morphology was observed. However, one series of measurements on the same powder pressed to different densities showed that there is an optimum density. Pressing the powder at about three atmospheres pressure increased the thermal conductivity at low pressures, indicating an increase in solid conduction. PPG was able to identify low cost modifications of their powders that had performance equal to or better than the more expensive commercially available powder that is the current industry standard for PEPs for use in the refrigerator industry.

2. MATERIALS SYNTHESIS AND CHARACTERIZATION

2.1 Synthesis of Silica Powders

The samples sent to ORNL were synthesized by traditional precipitation techniques. These techniques involved reacting sodium silicate and a mineral acid or carbon dioxide. The resulting precipitants were de-watered, washed, dried, and milled. A variety of parameters and operating conditions were controlled and varied to change the final product characteristics. Some samples contained non-silica powders or blends of silica and non-silica powders.

2.2 Characterization of Powders

The characteristics of the powders were determined by PPG Industries using a variety of techniques.

The particle size distribution of the powders was measured using a Coulter Multisizer (II Operating Procedure), using test method CD-25-42A. A sample is suspended in Isoton II (Coulter electrolyte) by stirring 10 minutes at 1000 rpm. An aliquot is withdrawn and pipetted into a second beaker of electrolyte. Particles from this stirred solution are drawn through a small orifice. The change in resistance of the solution is detected by platinum electrodes on either side of the orifice. The pulses produced are proportional to the volume of the particles. Volume and number distribution curves are produced. Particle sizes are given in units of microns.

The porosity was determined using test method CD-25-21. Using a Brabender plastograph, dibutylphthalate (DBP) is added to a dried sample in a mixing chamber while monitoring the torque. The end-point is taken from the torque vs. ml DBP graph. Units are cubic

centimeters per 100 grams.

The surface area (1-point) was measured using ASTM D1991.91. A dried sample (180°C) is degassed in a sample cell flushed with an inert atmosphere. In a 30% N_2/70% He atmosphere, the sample cell is submerged in liquid N_2 and a layer of nitrogen adsorbs on the silica surface. Upon removal from liquid N_2, the adsorbed N_2 is released, detected and reported as surface area. Units are square meters per gram.

The surface area (5-point) was measured using the CD 25-15B method. Surface area is determined in a similar manner to the 1-point Surface Area, except in this method, five pressure points are used to construct a curve. Surface area is then obtained from the curve. Again, units are square meters per gram.

The bulk density was measured using the CD 25-44 method. A portion of the sample is dropped (a few inches) into a sample cup of known volume so that an excess of powder is in the cup. The cup is tapped once, the powder is leveled to the top of the cup and the sample is weighed. Six replicates are run and the average is reported as bulk density. Units are grams per cubic centimeter.

The tap density was measured using the test method CD-25-44A. A portion of the sample is transferred to a cylinder and is tapped four times. A plunger is slowly and carefully inserted into the cylinder so that it just sits on the powder. This plunger height is subtracted from the zero height. Done in duplicate, this difference is calculated and reported as tap density. Again, units are grams per cubic centimeter.

[redacted]

To aid further in the characterization of the silicas, PPG agreed under confidentiality to provide additional characterizations of the silicas. These characterizations involved the use of mercury and nitrogen porosimetry. Mercury porosimetry was used to measure total intruded volume (cc/g), total pore surface area (m^2/g), and pore diameter (Angstroms). Nitrogen porosimetry was used to measure BET surface area (m^2/g), single point surface area (m^2/g), micro pore area (m^2/g), volume single point (cc/g), volume micro pore (cc/g), and average pore diameter (Angstroms). Some of these parameters were used in attempts to correlate material parameters with thermal data. However, due to the confidentiality of the data, none of the actual data are included in this report.

Based on thermal conduction theory and other information available from the literature, our goal was to provide very fine, light powders with high porosity. One shortcoming of the program was the inability to characterize the silica inside an evacuated panel. The silica became compressed inside the panel as it was exposed to atmospheric pressure. Therefore, the packing and porosity in between silica particles became as important as the porosity of the silica particles themselves. The mercury and nitrogen porosimetry data also had shortcomings. For example, nitrogen porosity is useful for pore sizes less than 1000 Angstroms, and mercury porosity utilizes high pressure which may collapse or distort the actual pore diameters.

2.3 Materials Tested

Four series of samples were prepared and studied in this program. The first series of samples was sent to ORNL in August of 1992. They included a variety of different silica based powders. A meeting was held in September at ORNL to discuss the scope of the project. At that

time, a decision was made to measure the thermal resistivity of the candidate powders in evacuated panels. Table 1 shows the characterization data of the first series of powders. The corresponding results seemed to be inconclusive (as discussed below). There was not a significant difference in resistivity between any of the silicas tested. Therefore, a different approach was used for the second series of samples. A meeting was held to discuss the results and it was decided to test the powders individually using a radial heat flow apparatus. This apparatus was designed to measure resistivity of powders at different pressures. Therefore, differences in resistivity at multiple pressures could be compared.

The second series of powders was sent to ORNL in December 1992. The samples are shown in Table 2. These samples were designed to compare some of the original samples using the two different resistivity measurement methods. Also, there were several blends of related samples to check particle size and packing phenomena. For example, BXS-420 and BXS-421 were blends of different particle size material made from the same silica base BXS-363. The results from this series indicated that the powder resistivities did not correlate well with the panel resistivity.

The third series included a variety of powders supplied to PPG by ORNL. These materials were analyzed, characterized and milled by PPG and returned to ORNL for thermal measurements. These samples were tested during the same time period as the second series samples. Included in these samples was Degussa FK500LS, a precipitated silica that has been used in the past and referred to in several patents on the subject. It was used as a standard to compare the results. Again, these samples were primarily measured using the radial heat flow apparatus. The characterizations for these samples are shown in Table 3.

Table 1. Characteristics of First Series of Powders

Name BXS-	Porosity (ml) (100g)	1 pt. Surface Area (m^2/g)	5 pt. Surface Area (m^2/g)	Bulk Density (g/cc)	Tap Density (g/cc)	Particle Size, microns Volume, % > 10	25	50	75	90	Particle Size, microns Population, % > 10	25	50	75	90
361	193	165	160	0.04	0.10	2.50	1.87	1.45	1.15	0.99	1.62	1.34	1.12	0.98	0.93
362	187	172	160	0.05	0.10	4.97	3.18	2.20	1.52	1.16	2.07	1.56	1.22	1.02	0.93
363	220	224	220	0.05	0.10	3.42	2.62	1.89	1.37	1.08	1.94	1.49	1.18	1.00	0.93
365	265	125	121	0.05	0.10	3.48	2.40	1.84	1.43	1.24	2.03	1.65	1.38	1.23	1.16
373	260	397	369	0.06	0.11	3.66	3.00	2.36	1.76	1.37	2.53	1.97	1.51	1.27	1.18
409	193	178	158	0.05	0.12	4.10	2.76	2.01	1.45	1.14	2.03	1.57	1.23	1.03	0.95
410	182	153	145	0.04	0.11	7.59	3.58	2.10	1.37	1.06	1.83	1.40	1.12	0.99	0.93

Table 2. Characteristics of Second Series of Powders

Name BXS-	Porosity (ml) (100g)	1 pt. Surface Area (m^2/g)	5 pt. Surface Area (m^2/g)	Bulk Density (g/cc)	Tap Density (g/cc)	Particle Size, microns Volume, % > 10	25	50	75	90	Particle Size, microns Population, % > 10	25	50	75	90
362	187	172	160	0.05	0.10	4.97	3.18	2.20	1.52	1.16	2.07	1.56	1.22	1.02	0.93
363	220	224	220	0.05	0.10	3.42	2.62	1.89	1.37	1.08	1.94	1.49	1.18	1.00	0.93
365	265	125	121	0.05	0.10	3.48	2.48	1.84	1.43	1.24	2.03	1.65	1.38	1.23	1.16
420	228	227	220	0.07	0.10	6.97	3.74	2.38	1.62	1.22	2.13	1.62	1.26	1.05	0.96
421	232	222	215	0.07	0.10	8.73	4.30	2.65	1.72	1.25	2.19	1.63	1.25	1.04	0.95
422	200	158	153	0.08	0.13	7.42	4.27	2.44	1.68	1.24	2.16	1.64	1.26	1.05	0.95
423	206	160	155	0.09	0.14	8.53	4.93	2.50	1.62	1.19	2.03	1.55	1.21	1.02	0.94
424	230	141	137	0.06	0.09	4.38	2.60	1.73	1.28	1.05	1.76	1.40	1.15	1.00	0.94
425	240	141	137	0.06	0.10	5.76	3.11	1.91	1.35	1.08	1.83	1.44	1.17	1.01	0.94
426	145	166	161	0.08	0.12	5.67	3.42	2.30	1.55	1.17	2.08	1.56	1.22	1.03	0.95
427	145	171	166	0.08	0.11	6.49	3.73	2.47	1.64	1.21	2.16	1.61	1.24	1.04	0.95
Y-121-3			609		0.22			15							
Y-129-2			625		0.12			3							
Y-129-3			426		0.14			2							

Table 3. Characteristics of Third Series of Powders

Name BXS-	Porosity (ml) (100g)	1 pt. Surface Area (m^2/g)	5 pt. Surface Area (m^2/g)	Bulk Density (g/cc)	Tap Density (g/cc)	Particle Size, microns Volume, % > 10	25	50	75	90	Particle Size, microns Population, % > 10	25	50	75	90
FK 500 LS	280	510	470	0.08	0.14	8.45	5.74	3.60	2.32	1.64	2.89	2.11	1.59	1.31	1.19
MH4Milled	123	368	260	0.18	0.32	5.076	3.44	2.54	1.87	1.40	2.49	1.92	1.43	1.12	0.98
Microcel E Milled	213	117	97	0.05	0.13	4.73	3.63	2.62	1.85	1.38	2.49	1.86	1.39	1.11	0.98
ME 80/20 Milled	231	93	80	0.05	0.13	8.40	4.98	3.10	1.99	1.40	2.42	1.77	1.32	1.07	0.96
Cabosil S17	275	353	328	0.08	0.10	28.51	19.72	13.01	8.16	5.82	9.44	6.88	4.87	3.60	3.08
MH2						32.71	23.81	14.36	7.70	4.10	4.71	2.99	2.07	1.67	1.52
MH3						46.81	32.62	17.06	7.66	3.97	5.28	3.67	2.76	2.31	2.13
MH4						26.53	20.35	13.66	7.64	4.13	5.88	3.89	2.83	2.34	2.14
Microcel E						29.48	20.62	15.33	11.21	6.89	9.57	5.04	3.21	2.47	2.19
ME 80/20						30.23	21.13	15.56	11.28	6.90	9.51	5.01	3.21	2.48	2.19
Mic Fly Ash	39	29	38	0.74	0.85	39.04	20.0	11.8	7.5	5.0	8.43	6.0	4.3	3.4	3.0

Table 4. Characteristics of Fourth Series of Powders

FK 500 LS	280	510	470	0.08	0.14	8.45	5.74	3.60	2.32	1.64	2.89	2.11	1.59	1.31	1.19
S_22LS	205	159	148	0.09	0.13	10.05	5.95	3.37	2.09	1.52	2.61	1.95	1.53	1.30	1.20
363-1	220	224	220	0.05	0.10	3.42	2.62	1.89	1.37	1.08	1.94	1.49	1.18	1.00	0.93
363-2	220	224	220	0.05	0.10	3.42	2.62	1.89	1.37	1.08	1.94	1.49	1.18	1.00	0.93
363-3	220	224	220	0.05	0.10	3.42	2.62	1.89	1.37	1.08	1.94	1.49	1.18	1.00	0.93
363-4	220	224	220	0.05	0.10	3.42	2.62	1.89	1.37	1.08	1.94	1.49	1.18	1.00	0.93
420	228	227	220	0.07	0.10	6.97	3.74	2.38	1.62	1.22	2.13	1.62	1.26	1.05	0.96
424	230	141	137	0.06	0.09	4.38	2.60	1.73	1.28	1.05	1.76	1.40	1.15	1.00	0.94
426	145	166	161	0.08	0.12	5.67	3.42	2.30	1.55	1.17	2.08	1.56	1.22	1.03	0.95
442	194	128	141	0.06	0.12	5.63	4.15	3.23	2.39	1.68	3.07	2.23	1.52	1.15	0.99
453	190	449	454	0.06	0.20	6.39	4.58	3.44	2.54	1.87	3.27	2.44	1.73	1.25	1.03
455	207	255	242	0.21	0.17	4.25	3.37	2.51	1.79	1.32	2.45	1.82	1.35	1.09	0.97
457	179	172	156	0.05	0.12	9.31	5.21	2.43	1.46	1.11	1.82	1.42	1.15	1.00	0.94
458	235	216	202	0.05	0.10	7.34	4.31	2.17	1.41	1.10	1.82	1.43	1.16	1.00	0.94
500	215	910	860	0.10	0.17	4.20	3.50	2.80	2.10	1.60	2.90	2.20	1.50	1.20	1.00
501	153	243	234	0.06	0.13	14.00	8.70	4.60	2.50	1.85	3.00	2.30	1.90	1.60	1.50

[redacted]

The fourth series of samples included the several samples from the earlier series as well as several new samples. The results from the first, second, and third series indicated that the radial heat flow apparatus gave biased results to the higher density powders. Therefore, a decision was made to use a new technique which was being developed by ORNL. It involved the ability to measure the thermal conductivity of panels at several pressures. The characterization data are shown in Table 4. The following table provides a brief description of these samples:

Sample	Description
FK500LS	Degussa silica
Sipernat 22 LS	Degussa silica
363-1	Initial high-R silica
363-2	Initial high-R silica, compressed to 15 psi before evacuation
363-3	Initial high-R silica, compressed to 50 psi before evacuation
363-4	Initial high-R silica, dried at 170°C
420	Blend of silicas
424	Blend of silicas
426	Blend of silica with low cost powder
442	Treated silica
453	Treated powder
455	New silica
457	New, low cost, silica
458	New silica
500	New, low cost, silica
501	New, low cost, silica

3. ORNL EXPERIMENTAL METHODS

3.1 Thermal Test Methods

Two thermal test apparatuses were used in this project. The first was a heat flow meter apparatus, which is shown schematically in Figure 1. This apparatus meets the specifications given in ASTM C 518. The apparatus was manufactured by Holometrix, Inc, and is an Rmatic Model R-41. The test specimen is sandwiched between two metal plates that are maintained at constant temperatures of 35.0°C (95°F) and 12.8°C (55°F), giving a mean specimen temperature of 23.9°C (75°F). For testing of powder evacuated panels, the panel was placed between two layers of fiberglass insulation and this package was placed between the hot and cold plates. This was done to protect both panels and the plates from any unintentional damage. Temperatures of the hot and cold sides of the evacuated panels were measured directly with thermocouples that were taped to the center of the Vecat outer bag. The heat flux through the specimen was measured with an array of 30 heat flux transducers that was placed on the lower (hot) plate. The two heat flux transducers in the center of the evacuated panel were used to obtain thermal resistance values. This gives a "center-of-panel" value that is not influenced by any heat flows around the edge of the panel. The heat flow meter apparatus is a comparative one; it is calibrated using standard reference materials from the National Institute of Standards and Technology. The uncertainty of the thermal resistance values obtained with the heat flow meter apparatus is about ±5 percent, and the precision of the data is about ±2.2 percent.

The value resulting from measurements in the heat flow meter apparatus is the thermal resistance of the test panel. A more meaningful value is the thermal resistivity, which is defined as

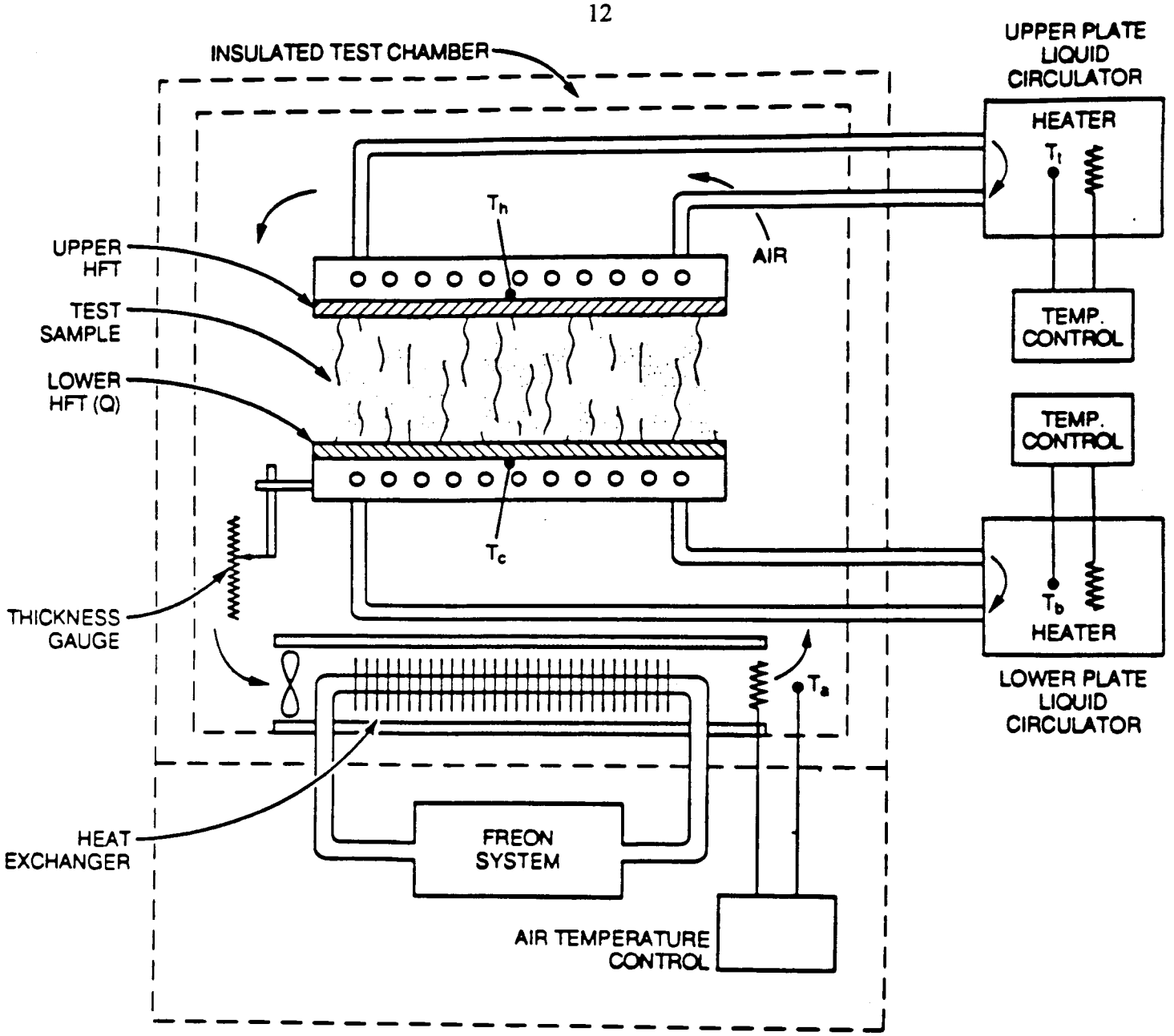

HFMA

Figure 1. Schematic of Heat Flow Meter Apparatus

the thermal resistance divided by the thickness of the panel. This gives a value that is the "R per inch" number. The panel thickness used for this calculation was measured at the center of the panel by the ORNL Inspection Department.

The other quantity that characterized the panel is the density. This quantity was measured by different techniques for the two types of powder evacuated panels. For the variable pressure powder evacuated panels, the mass of the powder was determined by weighing as it was added to the packages (described in another section), the thickness was measured by the Inspection Department as noted above, and the average length and width of the panel were measured with a steel rule. Because of the uneven edges of the panels, the length and width are the largest contributors to the overall uncertainty of the density values. This uncertainty is estimated at about the 10-15 percent level. The density of the evacuated panels that did not have a vacuum feedthrough was measured with a pycnometer method, that measures the volume of the panel by the displacement of water.

The other apparatus used for thermal tests was the radial heat flow apparatus (sometimes called the ORNL-7 apparatus). This is shown schematically in Figure 2. The powder specimen was contained in a brass tube with an inside diameter of 406 mm. The brass tube was wound with a copper cooling coil that was used to maintain the mean temperature of the specimen at about 27°C (81°F). The temperature of the brass tube was measured with three thermocouples. A thin-walled stainless steel tube with an outside diameter of 5.4 mm was placed along the axis of the brass cylinder and acted as a core heater. The stainless steel tube was heated by passing a direct electrical current through it. The temperature of the steel tube was measured using three thermocouples that were fed through the interior of the tube, out through tiny holes in the

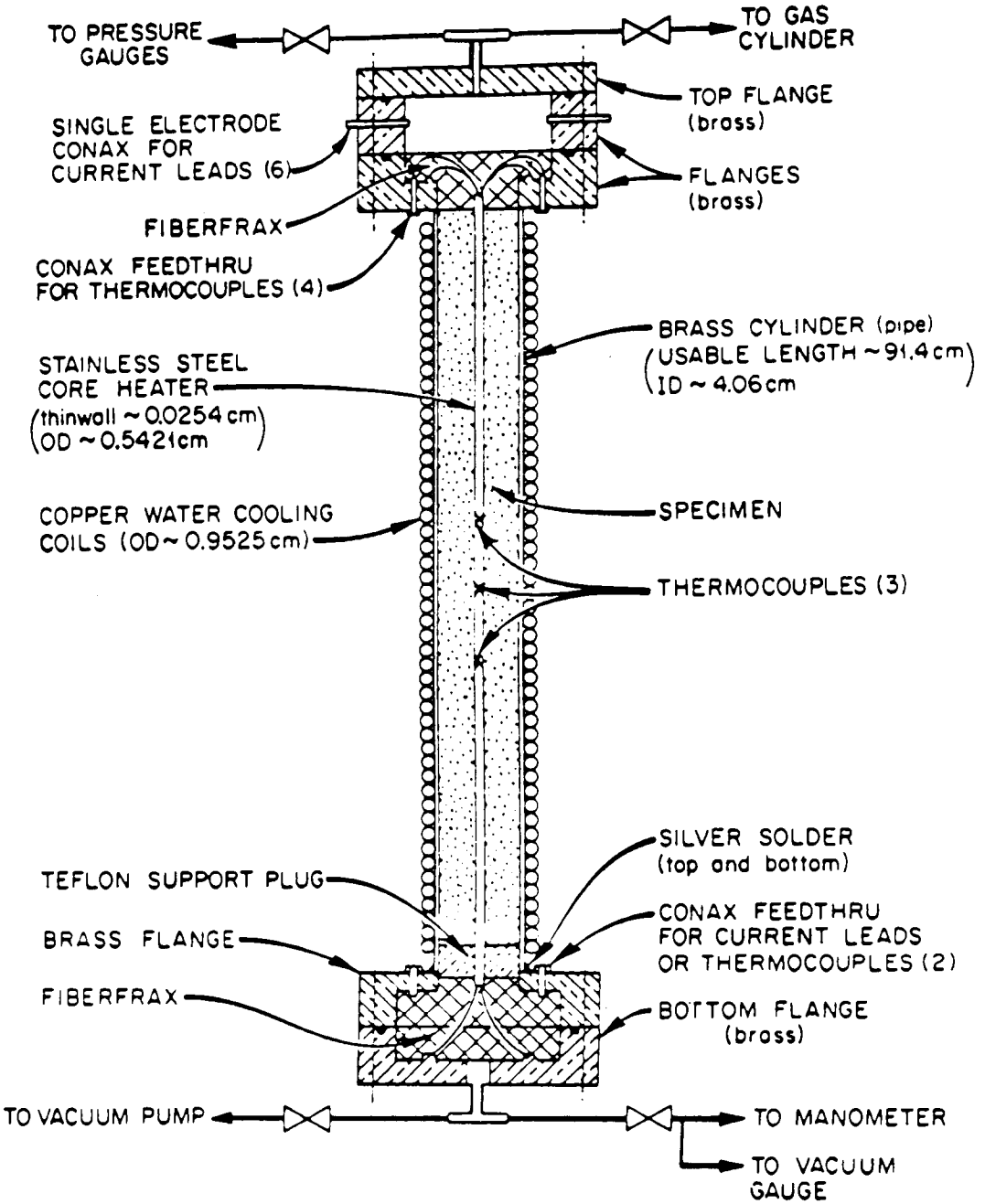

ORNL-7

Figure 2. Schematic of Radial Heat Flow Apparatus

tube, and were then spot-welded to the exterior surface of the tube. A drop of epoxy was used to protect the thermocouple junctions. The thermocouple wires served double duty of measuring the temperature of the tube as well as measuring the voltage drop along the central 102 mm section of the tube. This central 102 mm section formed the test section for the measurements, with the remaining lengths of core heater, brass outer tube, and powder serving as a guard against longitudinal heat flows. Since the heat input to the test section is measured directly from the current and voltage drop data, the apparatus is an absolute technique and does not rely upon calibration with standard reference materials. The uncertainty of the thermal resistivity values obtained with the radial heat flow apparatus is about ±3 percent and the precision of the data is about ±1.5 percent. The density of the powders in the radial heat flow apparatus was calculated from the mass of powder added to the apparatus and the known dimensions of the apparatus.

3.2 Preparation of Thermal Test Specimens

Three types of thermal test specimens were prepared from the powders that were studied in this project. The first type was a powder evacuated panel. The powders were first poured into a glass beaker and baked overnight in a drying oven that was set at 121°C (250°F) to remove adsorbed moisture. An inner bag approximately 254 mm (10 inches) square was made of a spun-bonded polyolefin film (Tyvek) which was also baked in the oven to remove plasticizers. The bag was heat sealed on three sides, the powder was poured into the bag, and the fourth side was heat sealed. An outer bag was made of a multilayer polymer film (Vecat), which was heat sealed on three sides. The inner bag containing the powder was placed inside the outer bag, and the assembly was placed in a Holymatic vacuum packer. The bags were weighted with lead weights,

the vacuum packer was evacuated to a pressure of slightly below 1 torr for one hour, and the fourth side of the outer bag was heat sealed under the vacuum.

The second type of specimen was powders at tapped density. Powders were baked overnight (or longer) at 121°C as was done for the powder evacuated panels. The powders were then poured slowly into the cylindrical annulus between the core heater and the outer tube of the radial heat flow apparatus. The outer tube was tapped with a rubber mallet as the powder was poured into it in order to avoid the creation of large voids within the test specimen. After the powder was poured into the apparatus, the tube containing the powder was slowly evacuated to the ultimate pressure of a mechanical vacuum pump (less than about 0.05 torr). The powder was then baked overnight at 110°C while it was under vacuum to remove any moisture that may have adsorbed onto the powder during the time period between removal from the baking oven and insertion into the radial heat flow apparatus.

The third type of specimen was variable pressure powder evacuated panels. Again the powders were baked out in the same manner as was done for the other two types of specimens. The powder was placed into a Tyvek inner bag which was heat sealed under atmospheric pressure. The inner bag was placed into a Vecat outer bag which was fitted with a perforated stainless pumping tube inside the bag and a vacuum feedthrough to connect it to an exterior valving and pumping system. After fabrication and final heat sealing of the outer bag, the pumping tube was connected to a mechanical vacuum pump and the panel was pumped overnight to a pressure of less than about 0.05 torr The panel was then valved off and inserted into the heat flow meter apparatus, where it was connected to another vacuum system that consisted of a mechanical vacuum pump, valves, and a capacitance manometer.

4. THERMAL TEST RESULTS

4.1 Initial Powder Evacuated Panels

The first series of thermal tests was conducted on evacuated panels that were made from seven powders furnished by PPG Industries. Results of tests on these panels are given in Table 5, where it is seen that the thermal resistivity values ranged from 24.4 to 28.0 $h \cdot ft^2 \cdot °F/Btu \cdot in$. These thermal resistivities are plotted against internal pressure in Figure 3, where the internal pressure measurements were made using ORNL's patented hand-held pressure gauge. For comparison, Figure 3 also shows thermal resistivity versus pressure data for FK500LS, as contained in the GE patent. These data indicate that the variations in thermal resistivity from one panel to another are likely to be due mainly to small differences in internal pressure. As shown in Figure 4, the variations in thermal resistivity have very little correlation with density.

Based on the results on the initial set of powder evacuated panels, the decision was made that it is necessary to be able to make thermal resistance measurements under controlled pressure conditions. The decision was made to conduct the next series of thermal tests in the radial heat flow apparatus where the pressure could be controlled from less than 0.1 torr to atmospheric pressure.

4.2 Powders Tested at Tapped Density

Twenty-five powders were tested in the radial heat flow apparatus. The powders were tested at tapped density, and curves of thermal resistivity versus pressure were generated. Powders tested included a commercial powder produced by PPG Industries (T-600), 15 experimental powders developed by PPG Industries (BXS-300, BXS-400, and Y 120 series), two

[redacted]

Table 5. Test Results on First Series of Evacuated Panels

Specimen	Thickness, mm	Density, g/cm^3	Temperature, °C	Pressure, Torr	Thermal Conductivity, W/m•K	Thermal Resistivity, h•ft^2•°F/Btu•in.
T600	8.192	0.205	24.27	4.0	0.005705	25.28
BXS-361	8.331	0.203	24.34	4.5	0.005340	27.01
BXS-363	8.865	0.197	24.31	3.0	0.005151	28.00
BXS-365	10.15	0.184	24.24	6.7	0.005329	27.07
BXS-373	10.22	0.186	24.23	7.5	0.005900	24.45
BXS-409	8.877	0.219	23.93	5.3	0.005536	26.06
BXS-410	9.322	0.203	24.33	3.3	0.005521	26.12

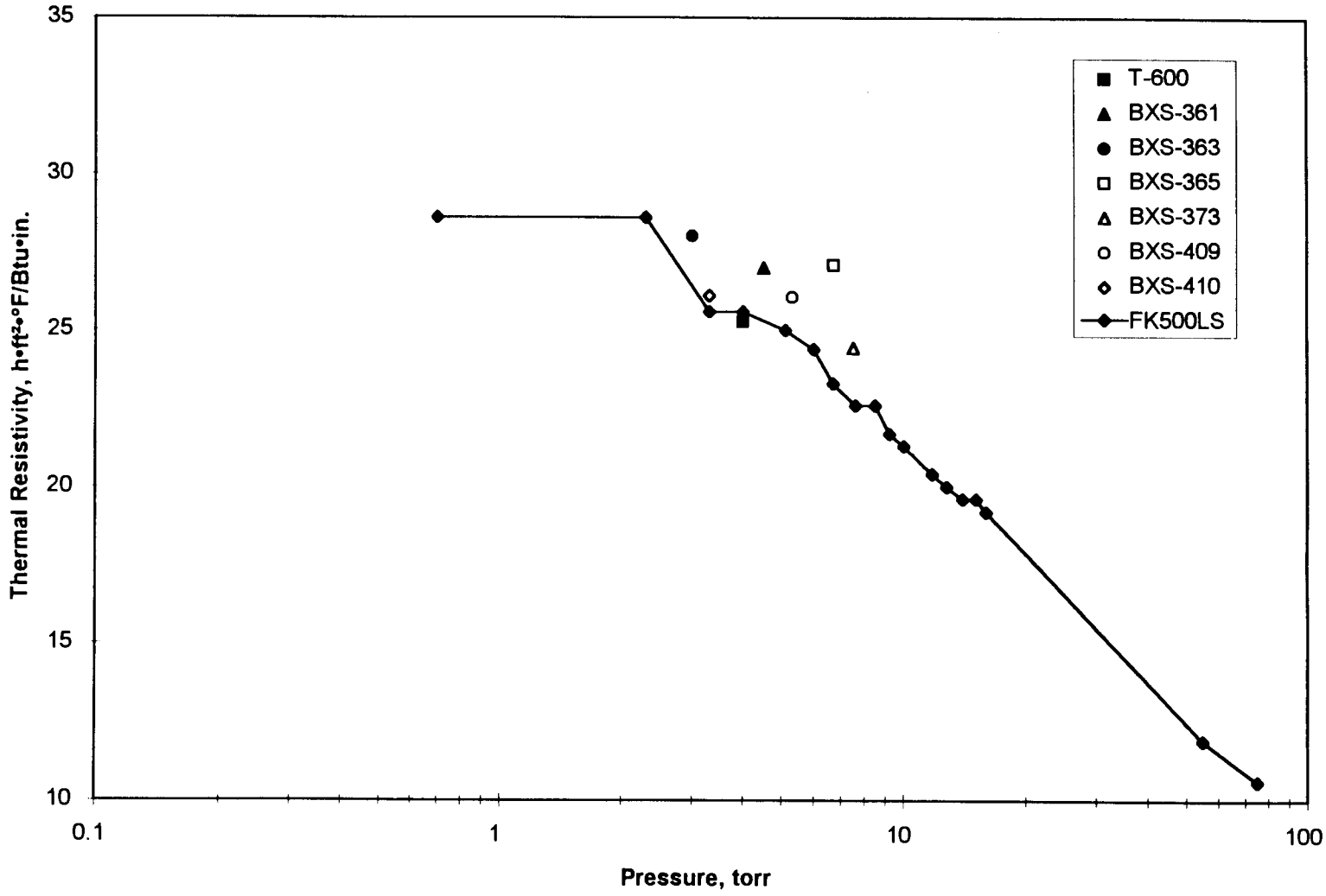

Figure 3. Test Results for First Series of Powder Evacuated Panels

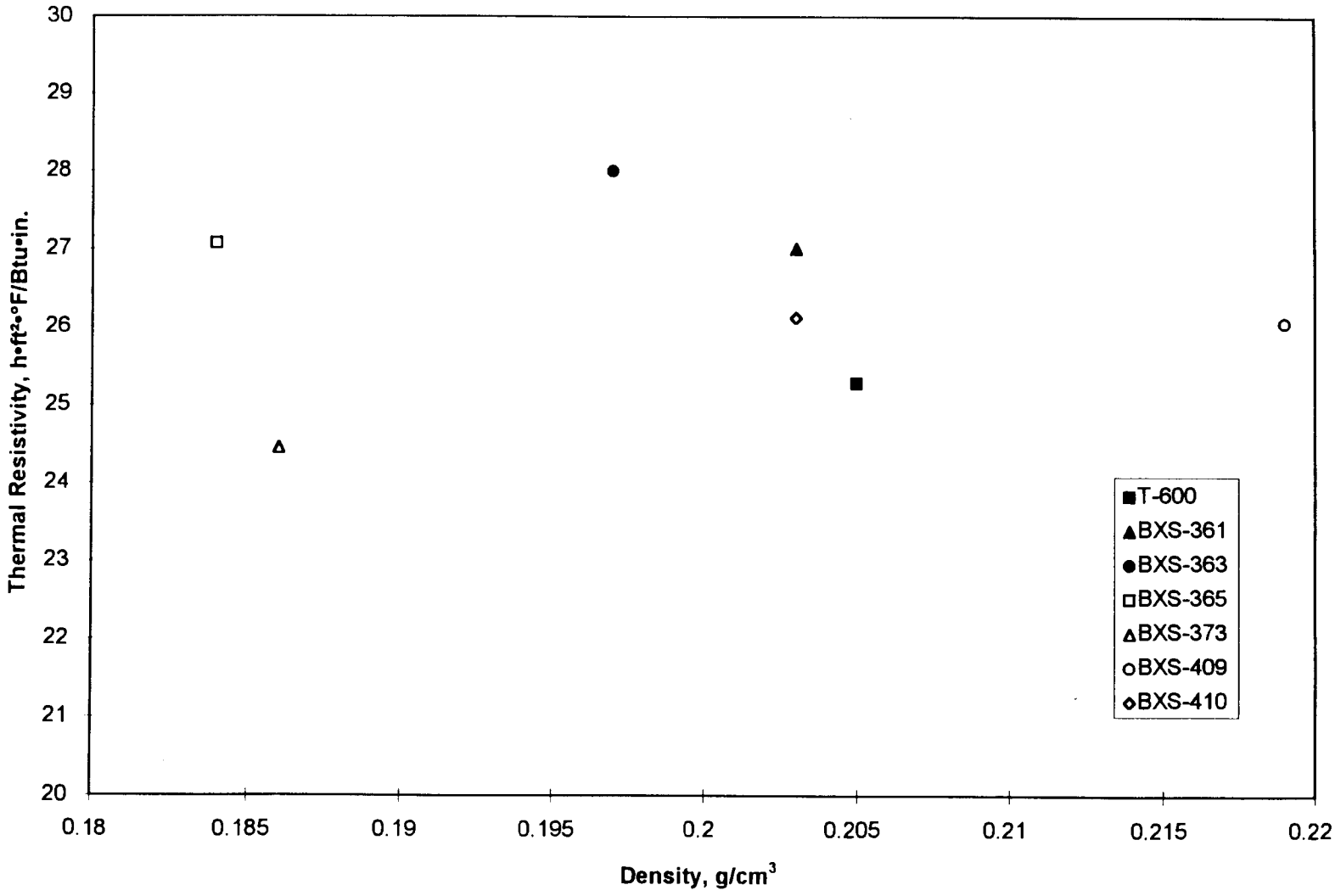

Figure 4. Effect of Density on Thermal Resistance of First Series of Powder Evacuated Panels

[redacted]

commercial powders produced by the Degussa Corporation (FK500LS and Sipernat 22 LS), two other commercial powders (Microcel E and Microcel 8020), a powder developed by ORNL, and fly ash powder from the Tennessee Valley Authority's Bull Run steam plant.

The data on the various powders are given in Tables 6 through 10. The data in these tables give the density of the powder as loaded into the radial heat flow apparatus, the pressure that was set in the apparatus using nitrogen gas, the measured thermal conductivity, and the R/in. value. Plots of thermal resistivity versus pressure are given in Figures 5 through 10.

Figure 5 shows the thermal resistivity of three commercially available powders. These include PPG's T-600 powder, and the two Degussa powders, FK500LS and Sipernat 22LS. Since FK500LS is currently the industry standard powder for producing PEPs, its curve of thermal resistivity versus pressure is used as a baseline on the remaining plots. As seen in Figure 5, the three commercial powders have similar characteristics, with the two Degussa powders having slightly better performance than the T-600 powder.

Figure 6 is a composite of the data measured on the experimental PPG powders that were labeled as BXS-300 and BXS-400 series. This shows that the best performance at pressures below 10 torr is obtained with BXS-454. At the lowest pressures, the thermal resistivity of BXS-454 was about 85 $h \cdot ft^2 \cdot °F/Btu \cdot in.$, which is about twice as high as that obtained with FK500LS. BXS-451 also had very high R-values at the lowest pressures, but the resistivity dropped off faster with increase in pressure than did that of BXS-454. The lowest resistivities were obtained with BXS-363. At the lowest pressures, the resistivity of BXS-363 was about one-half that of FK500LS. Only a few of the PPG powders were superior to the FK500LS. The data obtained on the BXS-300 and BXS-400 series of powders were examined in detail to determine whether the

[redacted]

Table 6. Results of Radial Heat Flow Apparatus Tests on PPG Powders at Tapped Density

Specimen	Density, g/cm^3	Pressure, torr	Thermal Conductivity W/m•K	Thermal Resistivity, $h•ft^2•°F/Btu/•in.$
T-600	0.073	0.072	0.003784	38.10
Specimen 1		1.93	0.005555	25.96
		4.08	0.006805	21.19
		9.76	0.009227	15.63
		20.10	0.01249	11.54
		50.80	0.0173	8.33
		102.5	0.02087	6.91
		503.9	0.02769	5.21
		763.5	0.02938	4.91

[redacted]

Table 6. Results of Radial Heat Flow Apparatus Tests on PPG Powders at Tapped Density (cont.)

Specimen	Density, g/cm^3	Pressure, torr	Thermal Conductivity W/m•K	Thermal Resistivity, h•ft^2•°F/Btu/•in.
BXS-363	0.053	0.075	0.006055	23.82
		0.087	0.004887	29.51
		0.17	0.006676	21.60
		0.593	0.008129	17.74
		1.56	0.009962	14.48
		5.44	0.01285	11.22
		9.83	0.01593	9.05
		19.15	0.01885	7.65
		99.85	0.0256	5.63
		489.2	0.03096	4.66
		783.2	0.03261	4.42
BXS-365	0.05	0.071	0.006083	23.71
		0.97	0.007626	18.91
		2.76	0.008706	16.56
		5.66	0.01042	13.83
		17.2	0.01504	9.58
		48.8	0.02004	7.20
		95.75	0.02339	6.16
		211.2	0.02676	5.39
		498.2	0.03007	4.80
		742.9	0.03121	4.62

[redacted]

Table 6. Results of Radial Heat Flow Apparatus Tests on PPG Powders at Tapped Density (cont.)

Specimen	Density, g/cm^3	Pressure, torr	Thermal Conductivity W/m•K	Thermal Resistivity, h•ft^2•°F/Btu/•in.
BXS-420	0.094	0.148	0.004592	31.40
		1.52	0.006613	21.80
		8.95	0.01125	12.82
		23.45	0.01522	9.47
		31.50	0.01660	8.69
		759.3	0.02944	4.90
BXS-421	0.078	0.160	0.005593	25.78
		1.39	0.008033	17.95
		9.11	0.01168	12.35
		32.10	0.01714	8.41
		760.8	0.02988	4.83
BXS-422	0.088	0.161	0.004273	33.74
		1.444	0.006611	21.81
		10.24	0.01222	11.80
		27.80	0.01658	8.70
		48.30	0.01923	7.50
		758.2	0.03366	4.28
BXS-423	0.086	0.186	0.003532	40.83
		1.53	0.004355	33.11
		10.40	0.008026	17.97
		22.75	0.01123	12.84
		752.7	0.02914	4.95

[redacted]

Table 6. Results of Radial Heat Flow Apparatus Tests on PPG Powders at Tapped Density (cont.)

Specimen	Density, g/cm^3	Pressure, torr	Thermal Conductivity W/m•K	Thermal Resistivity, h•ft^2•°F/Btu/•in.
BXS-424	0.065	0.275	0.004562	31.61
		0.382	0.004687	30.77
		1.39	0.006087	23.69
		9.50	0.009603	15.02
		34.70	0.01514	9.52
		35.10	0.01517	9.50
		756.1	0.03128	4.61
BXS-425	0.071	0.250	0.004134	34.88
		0.433	0.004839	29.80
		1.19	0.005897	24.46
		1.20	0.004666	30.91
		1.61	0.004426	32.58
		8.97	0.007146	20.18
		10.20	0.008692	16.59
		10.26	0.008625	16.72
		35.30	0.01315	10.97
		711.2	0.02800	5.15

[redacted]

Table 6. Results of Radial Heat Flow Apparatus Tests on PPG Powders at Tapped Density (cont.)

Specimen	Density, g/cm^3	Pressure, torr	Thermal Conductivity W/m•K	Thermal Resistivity, h•ft^2•°F/Btu/•in.
BXS-426	0.08	0.090	0.003687	39.11
		1.66	0.005800	24.86
		3.99	0.007098	20.31
		10.13	0.009836	14.66
		37.65	0.01532	9.42
		74.90	0.01884	7.65
		203.7	0.02204	6.54
		293.8	0.02450	5.88
		402.9	0.02614	5.52
		497.8	0.02702	5.34
		598.4	0.02786	5.18
		708.5	0.02855	5.05
		781.2	0.02846	5.07
		801.2	0.02905	4.96
		845.4	0.02890	4.99
		904.1	0.02924	4.93
		998.4	0.02964	4.86

[redacted]

Table 6. Results of Radial Heat Flow Apparatus Tests on PPG Powders at Tapped Density (cont.)

Specimen	Density, g/cm^3	Pressure, torr	Thermal Conductivity W/m•K	Thermal Resistivity, h•ft^2•°F/Btu/•in.
BXS-427	0.068	0.069	0.003629	39.74
		0.714	0.004486	32.15
		5.30	0.006144	23.47
		11.81	0.008360	17.25
		21.78	0.01051	13.72
		45.11	0.01393	10.35
		97.44	0.01834	7.86
		199.8	0.02268	6.36
		300.5	0.02507	5.75
		395.6	0.02661	5.42
		498.4	0.02779	5.19
		600.4	0.02875	5.02
		700.6	0.02949	4.89
		799.9	0.03015	4.78
		899.5	0.03060	4.71
		996	0.03110	4.64

[redacted]

Table 6. Results of Radial Heat Flow Apparatus Tests on PPG Powders at Tapped Density (cont.)

Specimen	Density, g/cm^3	Pressure, torr	Thermal Conductivity W/m•K	Thermal Resistivity, h•ft^2•°F/Btu/•in.
BXS-451	0.152	0.0865	0.001901	75.84
		0.2645	0.002865	50.33
		1.144	0.003855	37.40
		3.96	0.006146	23.46
		14.65	0.01214	11.88
		40.20	0.01959	7.36
		129.8	0.02828	5.10
		377.6	0.03524	4.09
		776.2	0.03852	3.74
BXS-454	0.105	0.0355	0.001700	84.82
		0.747	0.002445	58.98
		1.55	0.003077	46.87
		10.18	0.007610	18.90
		28.52	0.01258	11.46
		48.12	0.01619	8.90
		99.00	0.02144	6.73
		356.8	0.02706	5.33
		776	0.02943	4.90
Y 121-3	0.19	0.120	0.003557	40.54
		0.565	0.005550	25.98
		1.58	0.008636	16.70
		1.58	0.008711	16.55

[redacted]

Table 6. Results of Radial Heat Flow Apparatus Tests on PPG Powders at Tapped Density (cont.)

Specimen	Density, g/cm^3	Pressure, torr	Thermal Conductivity W/m•K	Thermal Resistivity, h•ft^2•°F/Btu/•in.
Y 129-2	0.105	745.2	0.03791	3.80
		745.3	0.03821	3.77
		0.049	0.002752	52.39
		0.681	0.004093	35.23
		1.66	0.005327	27.07
		6.82	0.008549	16.87
		21.62	0.01417	10.18
		104.6	0.02874	5.02
		752.6	0.03198	4.51
		997.4	0.03268	4.41
Y 129-3	0.117	0.128	0.002339	61.65
		2.34	0.003794	38.01
		8.98	0.007257	19.87
		25.08	0.01227	11.76
		73.40	0.01942	7.42
		149.6	0.02389	6.04
		990.4	0.03135	4.60

[redacted]

Table 7. Results of Radial Heat Flow Apparatus Tests on Degussa Powders at Tapped Density

Specimen	Density, g/cm^3	Pressure, torr	Thermal Conductivity W/m•K	Thermal Resistivity, h•ft^2•°F/Btu/•in.
FK500LS	0.088	0.180	0.003859	37.37
		0.780	0.003859	32.82
		2.30	0.004434	27.42
		4.80	0.005259	21.92
		9.95	0.006578	17.08
		12.45	0.009382	15.37
		19.55	0.01134	12.71
		20.15	0.0115	12.54
		41.85	0.01539	9.37
		97.80	0.02031	7.10
		98.20	0.02031	7.10
		755.1	0.03066	4.70
		759.4	0.03262	4.42
Sipernat 22LS	0.084	0.044	0.003351	43.04
		0.324	0.003695	39.03
		1.20	0.00443	32.55
		3.99	0.005931	24.31
		13.38	0.009101	15.84
		24.75	0.01164	12.39
		111.5	0.01752	8.23
		365.8	0.02425	5.95
		777.7	0.02814	5.12

Table 8. Results of Radial Heat Flow Apparatus Tests on Microcel Powders at Tapped Density

Specimen	Density, g/cm^3	Pressure, torr	Thermal Conductivity W/m•K	Thermal Resistivity, h•ft^2•°F/Btu/•in.
Microcel E	0.127	0.12	0.002855	50.50
		0.31	0.003212	44.90
		0.45	0.003745	38.50
		0.85	0.004383	32.90
		1.50	0.005934	24.30
		2.70	0.008793	16.40
		5.20	0.01222	11.80
		10.30	0.01752	8.23
		15.70	0.02090	6.90
		35.60	0.02731	5.28
		82.70	0.03277	4.40
Microcel E	0.043	0.026	0.002804	51.42
Micronized		0.050	0.002891	49.88
		0.068	0.002982	48.35
		0.191	0.003297	43.74
		1.48	0.004866	29.64
		5.01	0.007549	19.10
		10.59	0.01092	13.21
		53.8	0.02007	7.18
		742	0.03556	4.06

[redacted]

Table 8. Results of Radial Heat Flow Apparatus Tests on Microcel Powders at Tapped Density (cont.)

Specimen	Density, g/cm^3	Pressure, torr	Thermal Conductivity W/m•K	Thermal Resistivity, $h•ft^2•°F/Btu/•in.$
Microcel 8020	0.052	0.026	0.002500	57.68
Micronized		0.256	0.003273	44.06
		1.01	0.003921	36.78
		4.69	0.006880	20.96
		12.00	0.01057	13.64
		50.01	0.01872	7.70
		101.4	0.02362	6.10
		503.1	0.03029	4.76
		759.3	0.03194	4.52

Table 9. Results of Radial Heat Flow Apparatus Tests on ORNL Powder at Tapped Density

Specimen	Density, g/cm^3	Pressure, torr	Thermal Conductivity W/m•K	Thermal Resistivity, h•ft^2•°F/Btu/•in.
MH-4 Powder		0.54	0.002139	67.40
Unmicronized		0.95	0.002916	49.45
		2.10	0.003783	38.12
		3.10	0.005251	27.46
		4.20	0.007188	20.06
		4.90	0.007618	18.93
		6.30	0.008996	16.03
		7.50	0.01017	14.18
		8.30	0.01075	13.41
		14.50	0.01590	9.07
MH-4	0.175	0.043	0.002994	48.16
Micronized		0.500	0.003784	38.10
		1.11	0.004189	34.42
		7.06	0.007138	20.20
		20.10	0.01109	13.00
		43.55	0.01575	9.16
		56.90	0.01791	8.05
		106.2	0.02249	6.41
		380.8	0.03194	4.51
		756.5	0.03584	4.02

Table 10. Results of Radial Heat Flow Apparatus Tests on Fly Ash at Tapped Density

Specimen	Density, g/cm^3	Pressure, torr	Thermal Conductivity W/m•K	Thermal Resistivity, $h•ft^2•°F/Btu/•in.$
Treated	0.702	0.044	0.003156	45.69
		0.521	0.004725	30.52
		1.54	0.009418	15.31
		10.11	0.03129	4.61
		103.7	0.08326	1.73
		771.7	0.1156	1.25
Sieved	0.716	0.037	0.001708	84.42
		0.038	0.001694	85.12
		0.105	0.002745	52.53
		0.315	0.003105	46.44
		0.977	0.005361	26.90
		4.18	0.01770	8.15
		7.75	0.02666	5.41
		10.05	0.03115	4.63
		23.65	0.04964	2.90
		40.85	0.06345	2.27
		91.00	0.08210	1.756
		345.9	0.1055	1.367
		766.4	0.1384	1.042

Table 10. Results of Radial Heat Flow Apparatus Tests on Fly Ash at Tapped Density (cont.)

Specimen	Density, g/cm^3	Pressure, torr	Thermal Conductivity W/m•K	Thermal Resistivity, $h•ft^2•°F/Btu/•in.$
Micronized	0.833	0.210	0.002043	70.57
		1.03	0.003190	45.20
		2.26	0.005025	28.70
		3.74	0.006343	22.73
		8.99	0.01205	11.96
		22.80	0.02268	6.36
		55.55	0.04120	3.50
		326.2	0.09250	1.559
		740.8	0.1195	1.207
		742.5	0.1198	1.204

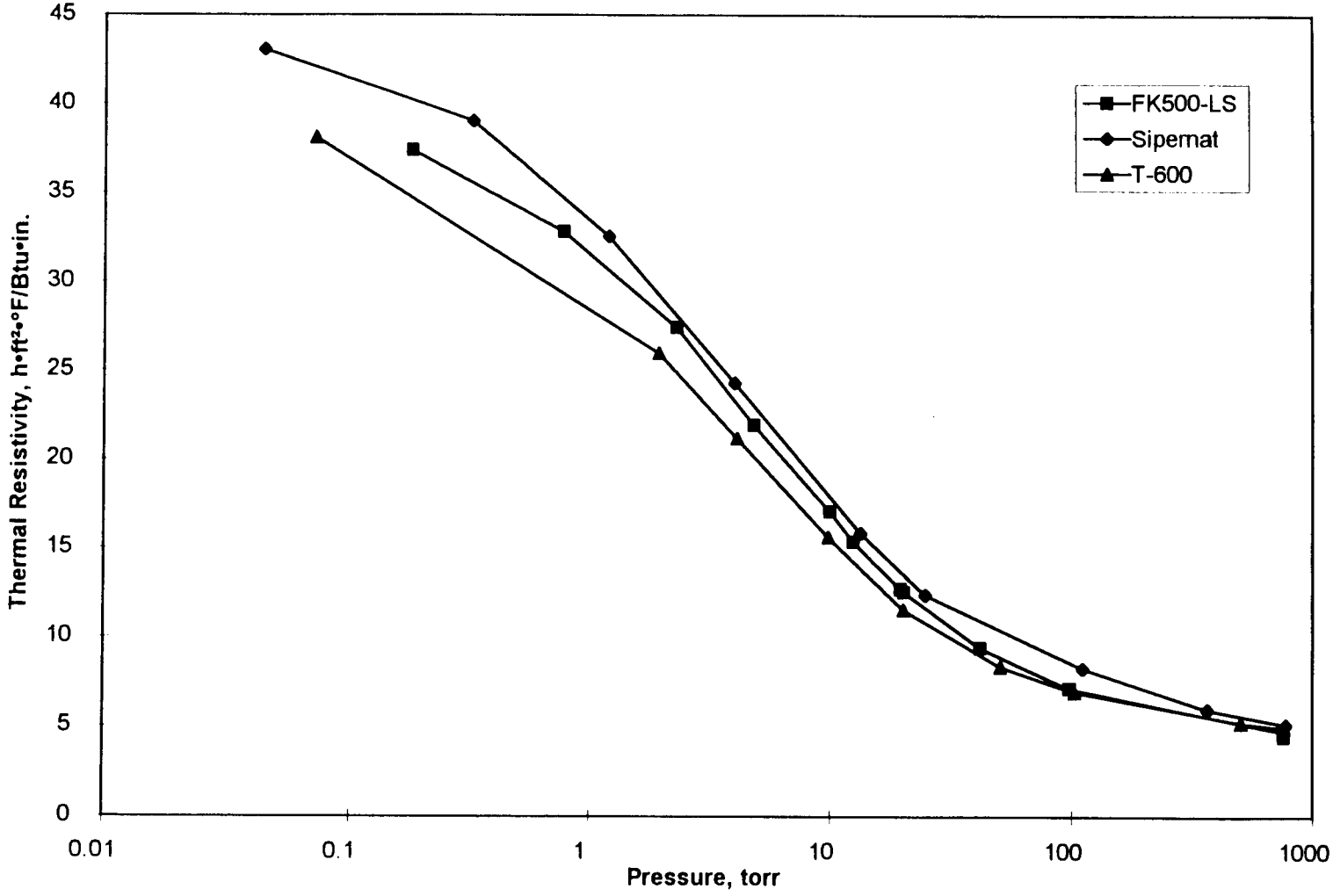

Figure 5. Thermal Resistivity of Commercial Powders at Tapped Density

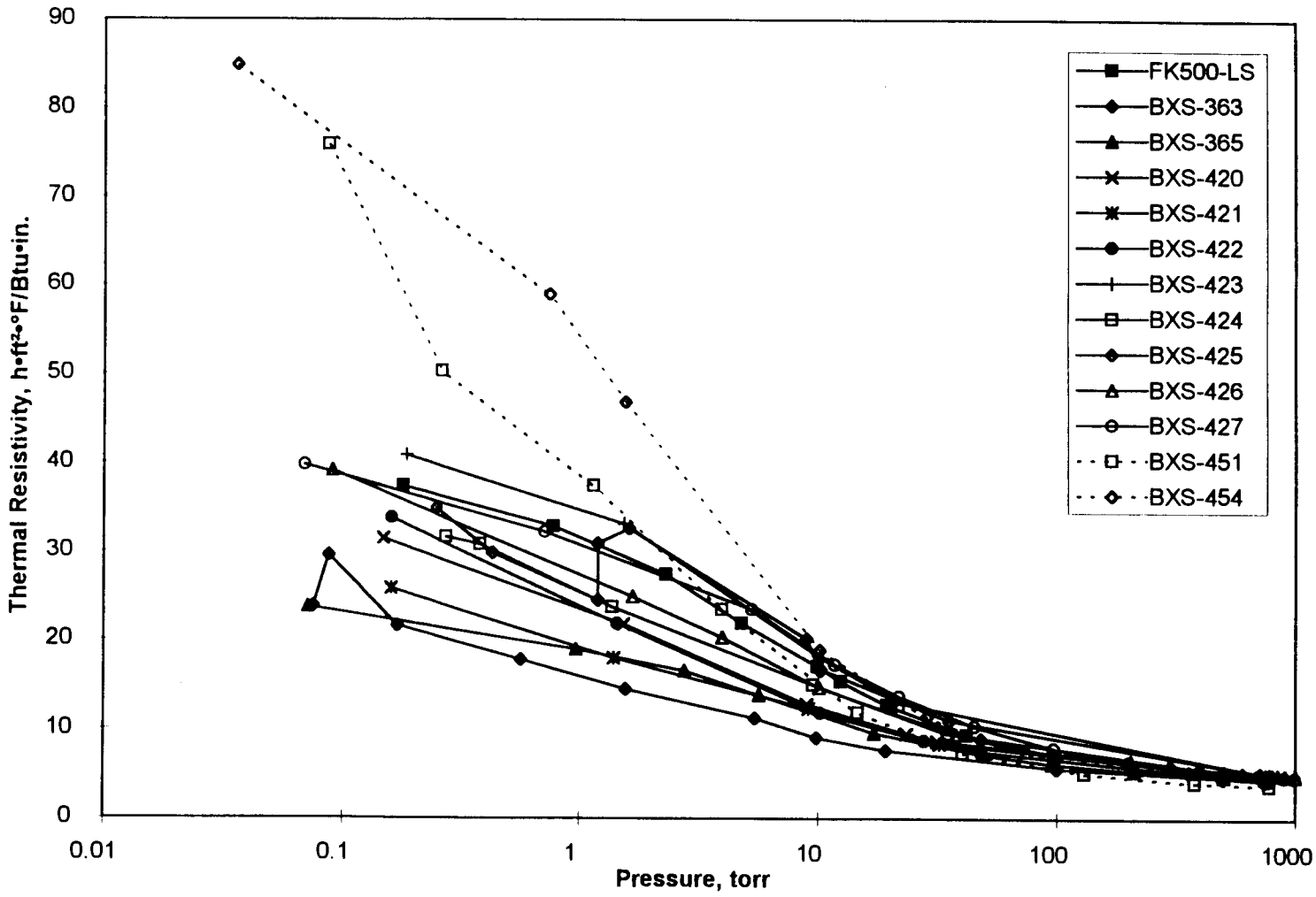

Figure 6. Thermal Resistivity of PPG Series 300 and 400 Powders at Tapped Density

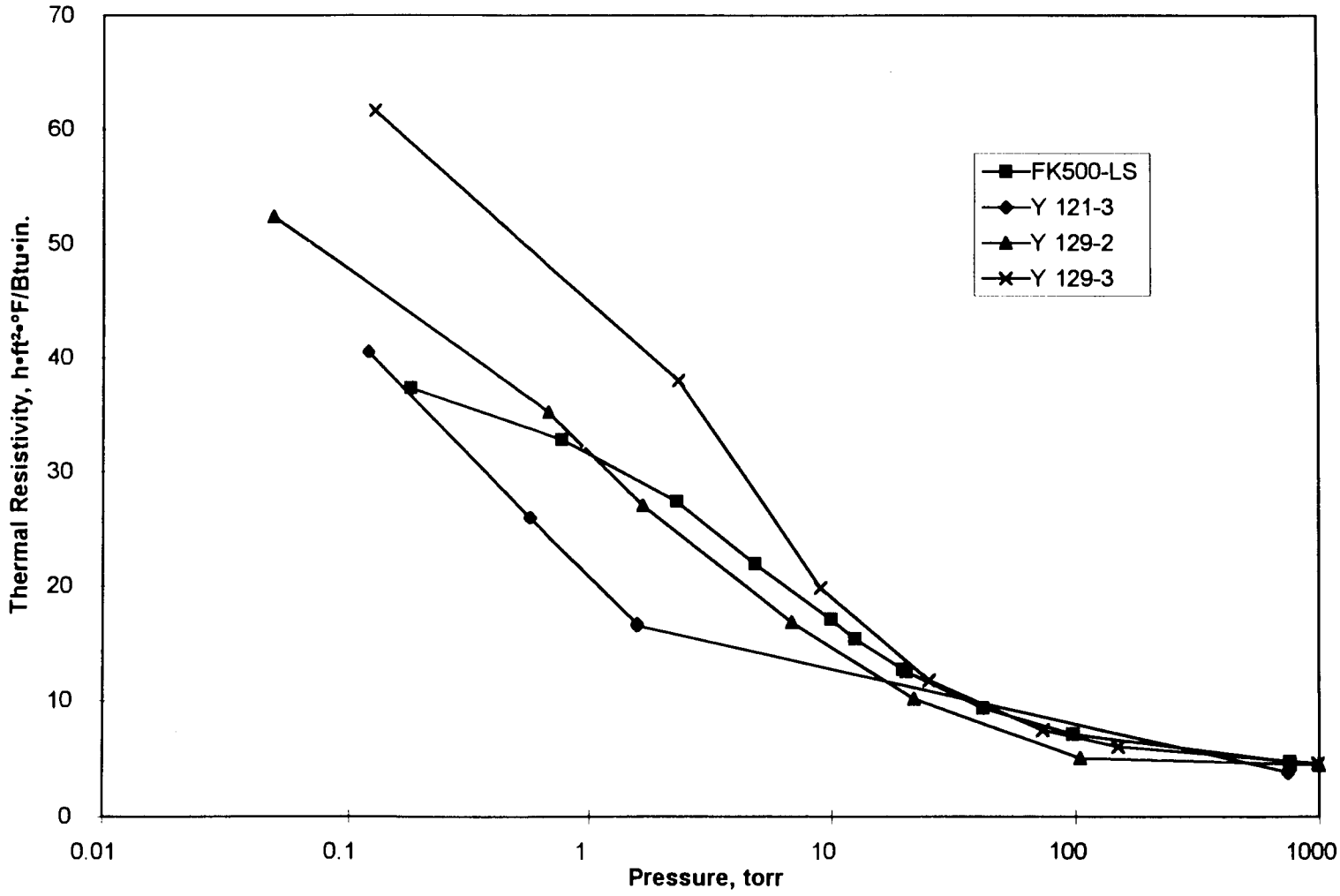

Figure 7. Thermal Resistivity of PPG Series Y Powders at Tapped Density

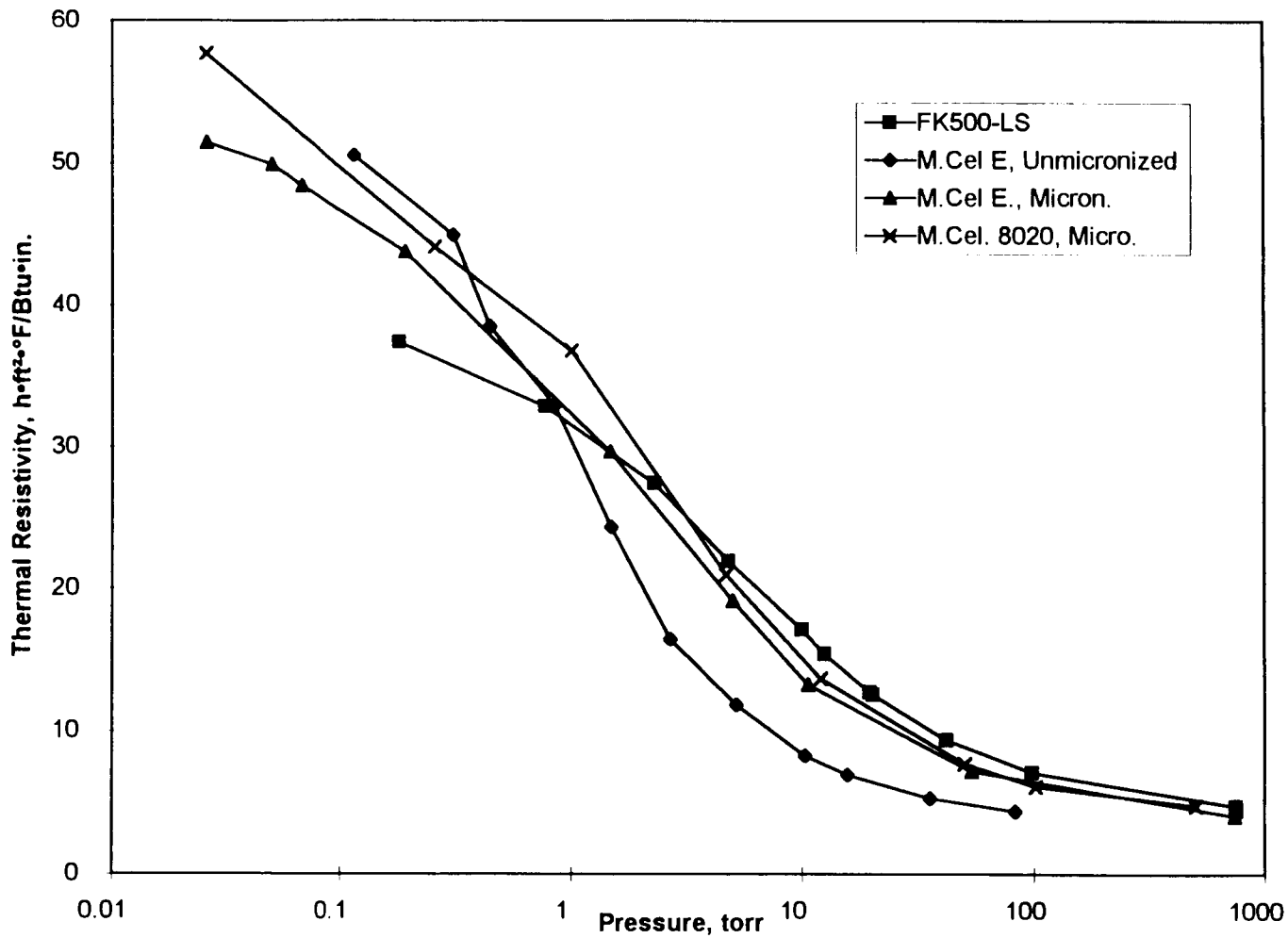

Figure 8. Thermal Resistivity of Microcel Powders at Tapped Density

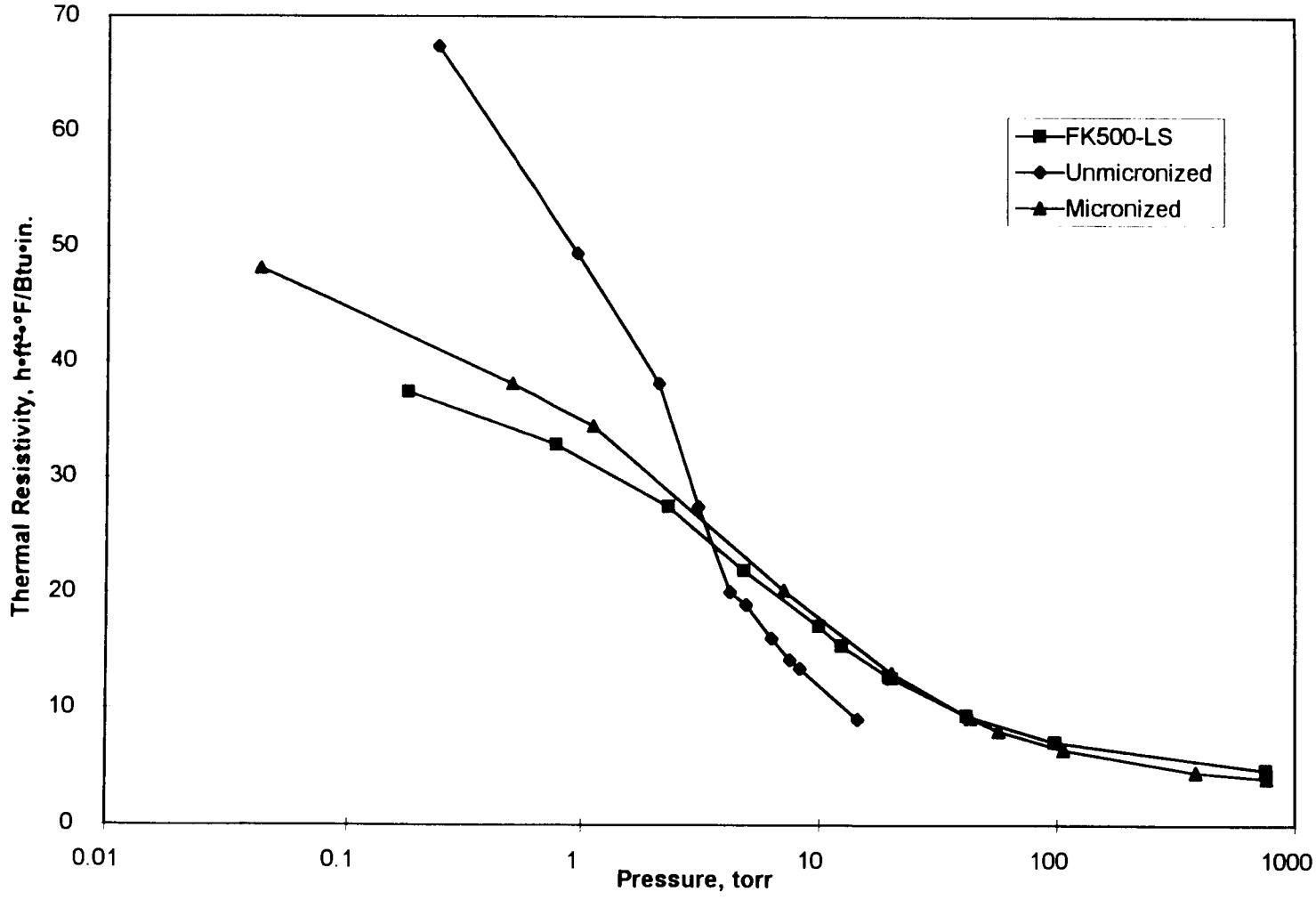

Figure 9. Thermal Resistivity of ORNL Powder at Tapped Density

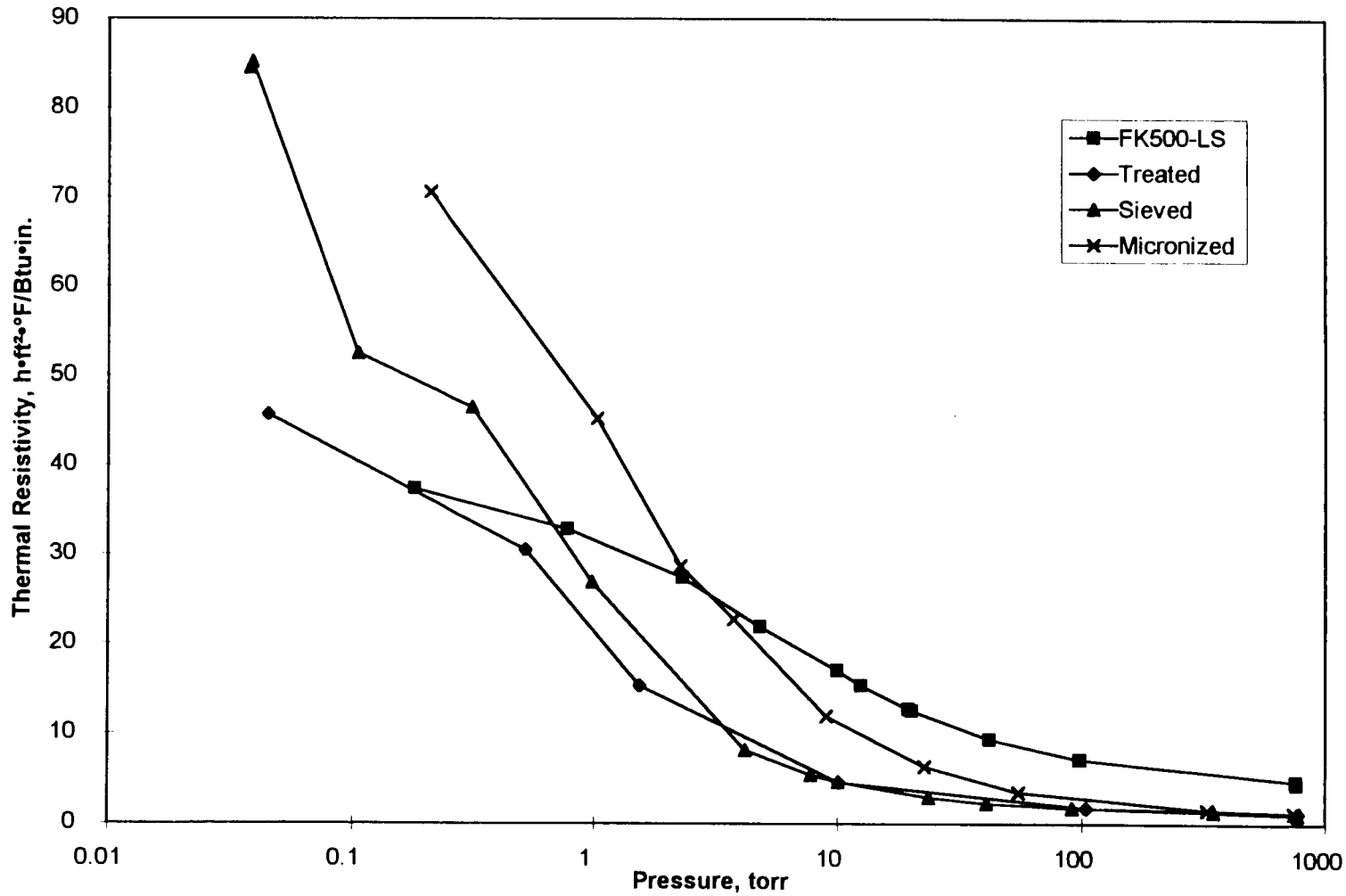

Figure 10. Thermal Resistivity of Fly Ash at Tapped Density

[redacted]

thermal data could be correlated with data that were obtained on powder characteristics. Discussion of these correlations is given in a later section of the report.

Figure 7 shows the data obtained on the PPG Y series of powders, and a comparison with FK500LS. At the lowest pressures, all three Y powders had resistivities greater than that of FK500LS. The highest resistivity was obtained with Y 129-3, which had a resistivity higher than that of FK500LS over most of the pressure range.

Data obtained on Microcel powders are given in Figure 8. Two types of Microcel powders were studied, Microcel E and Microcel 80/20. Microcel E was measured in the as-received condition and after particle size reduction by micronization. Micronization of the Microcel E powder changed its mean particle diameter from 5.56 microns to 1.7 microns. For the Microcel 80/20, micronization changed the particle size from 5.53 to 1.63 microns. At pressures below about 1 torr, micronization lowered the thermal resistivity. Above 1 torr, micronization improved the resistivity.

A powder developed at ORNL was measured both before and after micronization (see Figure 9). The effect of micronization was to change the mean particle diameter from 3.8 to 1.7 microns. At pressures below about 3 torr, the resistivities of both the unmicronized and micronized powders were better than FK500LS. Below this pressure, the unmicronized powder had a higher resistivity, but above this pressure, the micronized powder was superior.

Specimens of fly ash obtained from TVA's Bull Run Steam Plant were studied in the heat flow meter apparatus. The specimens had been treated by ORNL's Chemical Technology Division to remove heavy metals. One specimen was measured as-treated. Another was measured after sieving to remove the largest particles, and a third specimen was measured after micronization.

Data obtained on three specimens of fly ash are given in Figure 10. These data show that particle size reduction by micronization shifts the resistivity-pressure curve to the right (towards higher pressures). Below about 2 torr, the resistivity of micronized fly ash is superior to that of FK500LS. However, the densities of the fly ash specimens were nearly an order of magnitude higher than that of FK500LS.

4.3 Variable Pressure Powder Evacuated Panels

Fourteen variable pressure powder evacuated panels were measured in the heat flow meter apparatus to generate curves of thermal resistivity versus pressure. Powders used for these panels included two commercial powders produced by Degussa Corp. (FK500LS and Sipernat 22LS) and nine experimental powders developed by PPG Industries.

Data on the fourteen panels are given in Tables 11 and 12, and are plotted on the composite graph in Figure 11. At low pressures, the thermal resistivities of the panels made from the PPG powders varied from 24.3 to 32.3 $h \cdot ft^2 \cdot °F/Btu \cdot in$. For comparison, the panels made from FK500LS and Sipernat 22LS had low pressure resistivities of 28.6 and 31.2 $h \cdot ft^2 \cdot °F/Btu \cdot in$., respectively. As the normalized plot in Figure 12 shows, the resistivity of the panels is essentially independent of pressure up to about 2 torr, and then decreases with increasing pressure.

Results obtained on four panels made with BXS-363 powder are shown in Figure 13, along with the corresponding data on the powder at tapped density. The first panel was made as described above. The second was pressed in a hydraulic press to 15 psi and then evacuated. The third panel was pressed to 50 psi and then evacuated. The fourth panel was made the same way as the first panel, except that the powder was dried at 170°C instead of 121°C. The first and

[redacted]

Table 11. Results of Heat Flow Meter Apparatus Measurements of Variable Pressure PEPs made with PPG Powders

Specimen	Thickness, mm	Density, g/cm^3	Pressure, torr	Thermal Conductivity, W/m•K	Thermal Resistivity, h•ft^2•°F/Btu•in.
BXS-363	7.47	0.19	0.26	0.004614	31.25
			1.06	0.004766	30.26
			2.80	0.004959	29.08
			6.00	0.005314	27.14
			11.22	0.006065	23.78
			20.21	0.007080	20.37
			84.89	0.01181	12.21
BXS-363 (2)	14.10	0.180	0.17	0.004888	29.50
			1.37	0.004969	29.02
			6.39	0.005559	25.94
			20.39	0.007008	20.58
			86.18	0.0125	12.82
BXS-363 (3)	14.12	0.209	0.03	0.005863	24.30
			0.12	0.005860	24.61
			1.74	0.006026	23.93
			6.00	0.006613	21.80
			10.42	0.006780	21.27
			23.57	0.007899	18.26
			24.10	0.007878	18.30
			86.37	0.01153	12.51
BXS-363 (4)	12.01	0.194	0.09	0.004492	32.10
			2.17	0.004694	30.72
			10.20	0.005863	24.60
			20.94	0.007070	20.40

[redacted]

Table 11. Results of Heat Flow Meter Apparatus Measurements of Variable Pressure PEPs made with PPG Powders (cont.)

Specimen	Thickness, mm	Density, g/cm^3	Pressure, torr	Thermal Conductivity, W/m•K	Thermal Resistivity, h•ft^2•°F/Btu•in.
BXS-363 (4)			85.78	0.01184	12.18
BXS-424	17.18	0.187	0.11	0.004490	32.11
			1.88	0.004963	29.05
			8.95	0.006049	23.84
			17.07	0.007337	19.65
			71.61	0.01209	11.93
BXS-426	24.55	0.225	0.13	0.004459	32.34
			3.02	0.005318	27.12
			10.93	0.007028	20.52
			13.46	0.007100	20.29
			22.18	0.008088	17.83
			91.31	0.01344	10.73
BXS-442	12.58	0.207	0.17	0.004813	29.96
			1.24	0.004924	29.28
			6.12	0.005580	25.84
			19.66	0.007100	20.31
			88.38	0.01205	11.97
BXS-450	12.17	0.300	0.48	0.005980	24.11
			1.46	0.006117	23.57
			10.52	0.008555	16.86
			27.50	0.01232	11.71
			85.92	0.01873	7.70

[redacted]

Table 11. Results of Heat Flow Meter Apparatus Measurements of Variable Pressure PEPs made with PPG Powders (cont.)

Specimen	Thickness, mm	Density, g/cm^3	Pressure, torr	Thermal Conductivity, W/m•K	Thermal Resistivity, h•ft^2•°F/Btu•in.
BXS-453	8.99	0.308	0.21	0.005209	27.68
			1.21	0.005350	26.95
			6.31	0.006809	21.18
			20.49	0.01001	14.41
			89.49	0.01843	7.82
BXS-455	12.01	0.236	0.41	0.005680	25.39
			2.16	0.006157	23.42
			12.17	0.008383	17.20
			20.40	0.009807	14.70
			78.35	0.01615	8.93
BXS-457	11.32	0.252	0.13	0.004870	29.61
			2.31	0.005098	28.28
			6.40	0.005754	25.06
			16.51	0.006819	21.15
			91.44	0.01268	11.37
BXS-458	12.78	0.189	0.06	0.004676	30.84
			2.28	0.005015	28.76
			9.13	0.007454	19.34
			23.58	0.008917	16.17
			83.93	0.01310	11.01

Table 12. Results of Heat Flow Meter Apparatus Measurements of Variable Pressure PEPs made with Degussa Powders

Specimen	Thickness, mm	Density, g/cm^3	Pressure, torr	Thermal Conductivity, W/m•K	Thermal Resistivity, h•ft^2•°F/Btu•in.
FK500LS	13.00	0.185	0.03	0.005044	28.59
			1.28	0.005315	27.13
			4.36	0.006627	21.76
			12.90	0.008867	16.26
			20.94	0.01062	13.58
			51.28	0.01480	9.75
			77.44	0.01707	8.45
Sipernat 22LS	12.46	0.211	0.10	0.004628	31.16
			2.25	0.004675	30.84
			9.79	0.006029	23.92
			23.97	0.007620	18.92
			79.92	0.01193	12.08

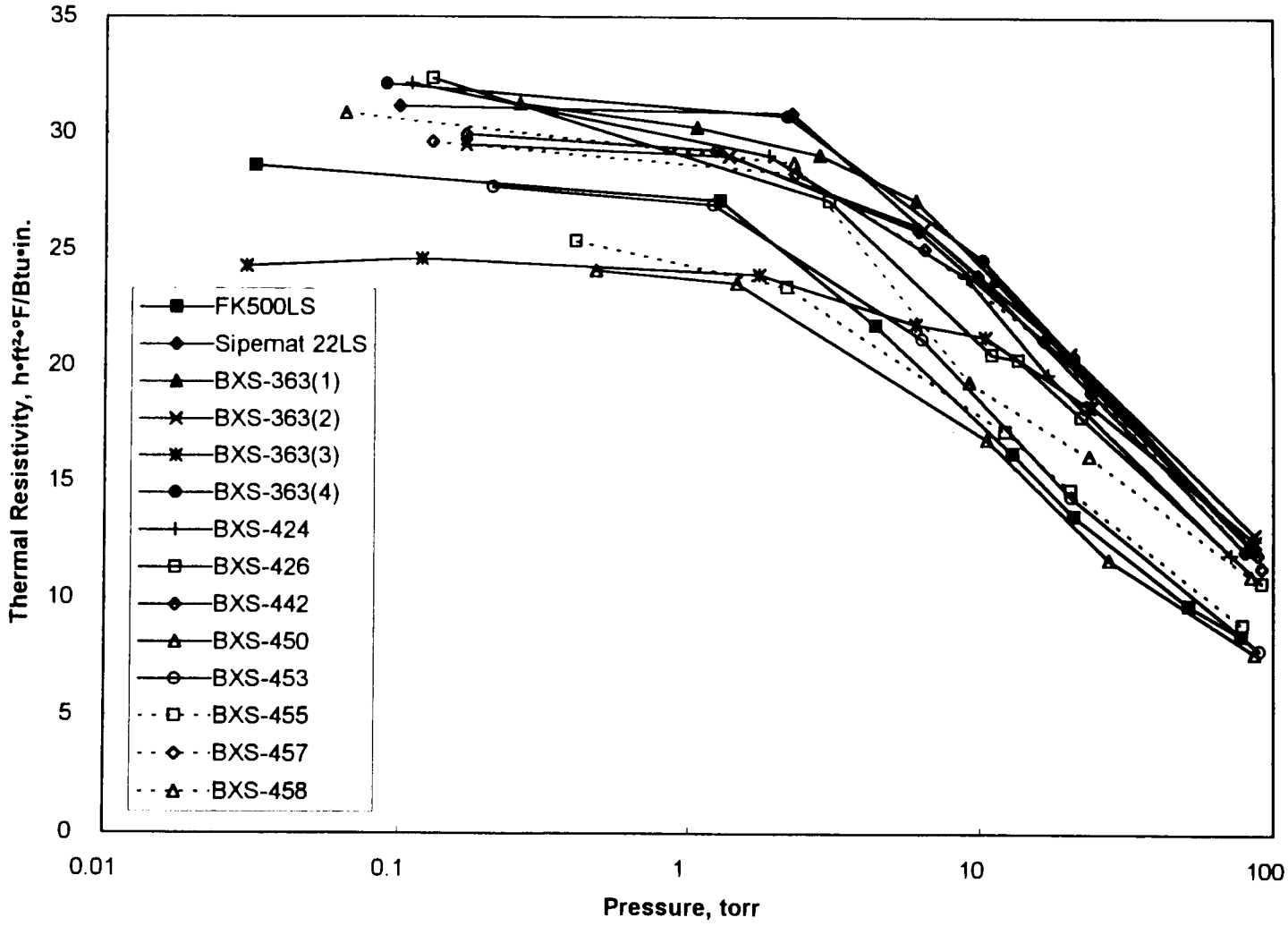

Figure 11. Thermal Resistivity of Variable Pressure Powder Evacuated Panels

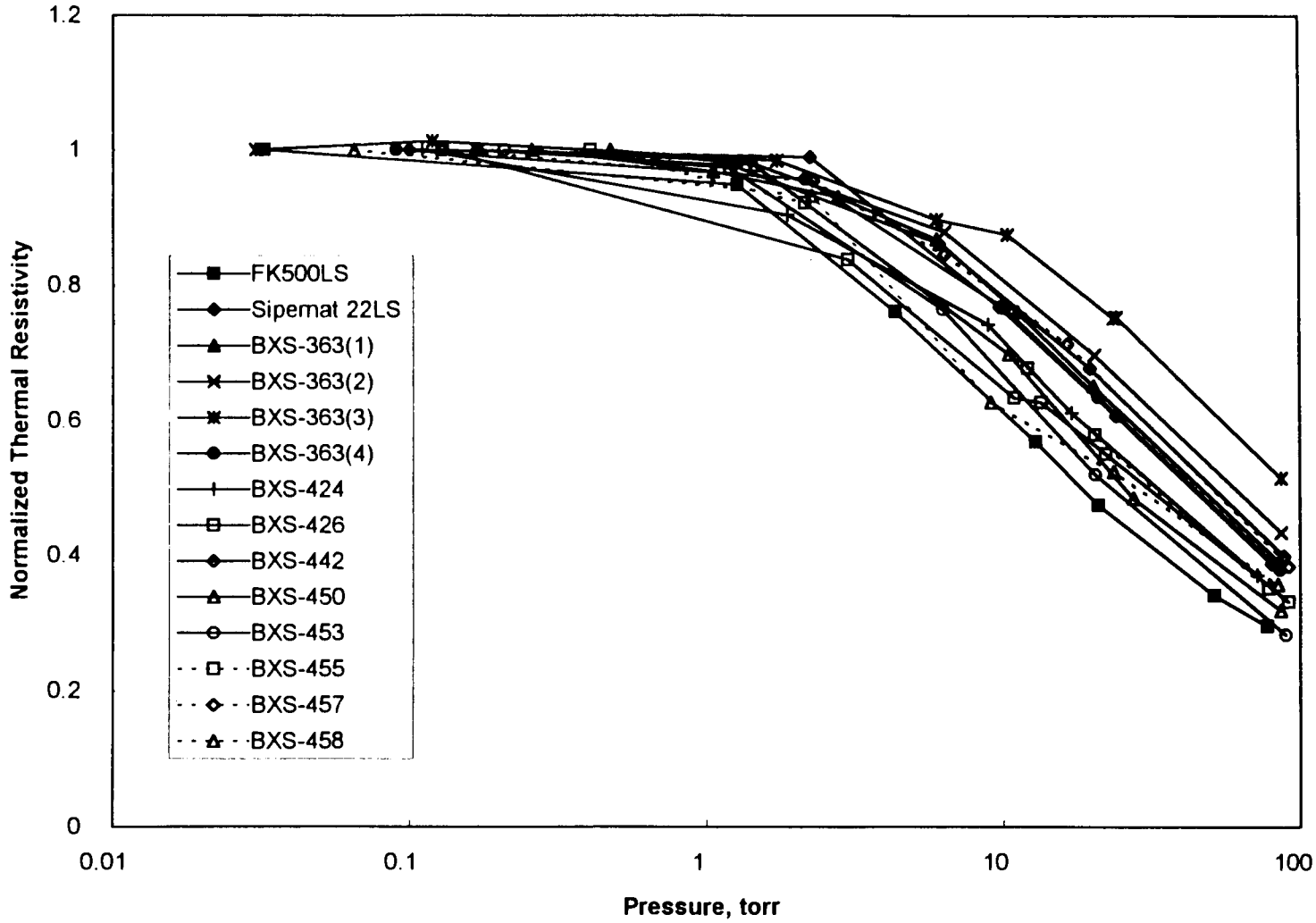

Figure 12. Normalized Thermal Resistivity of Variable Pressure Powder Evacuated Panels

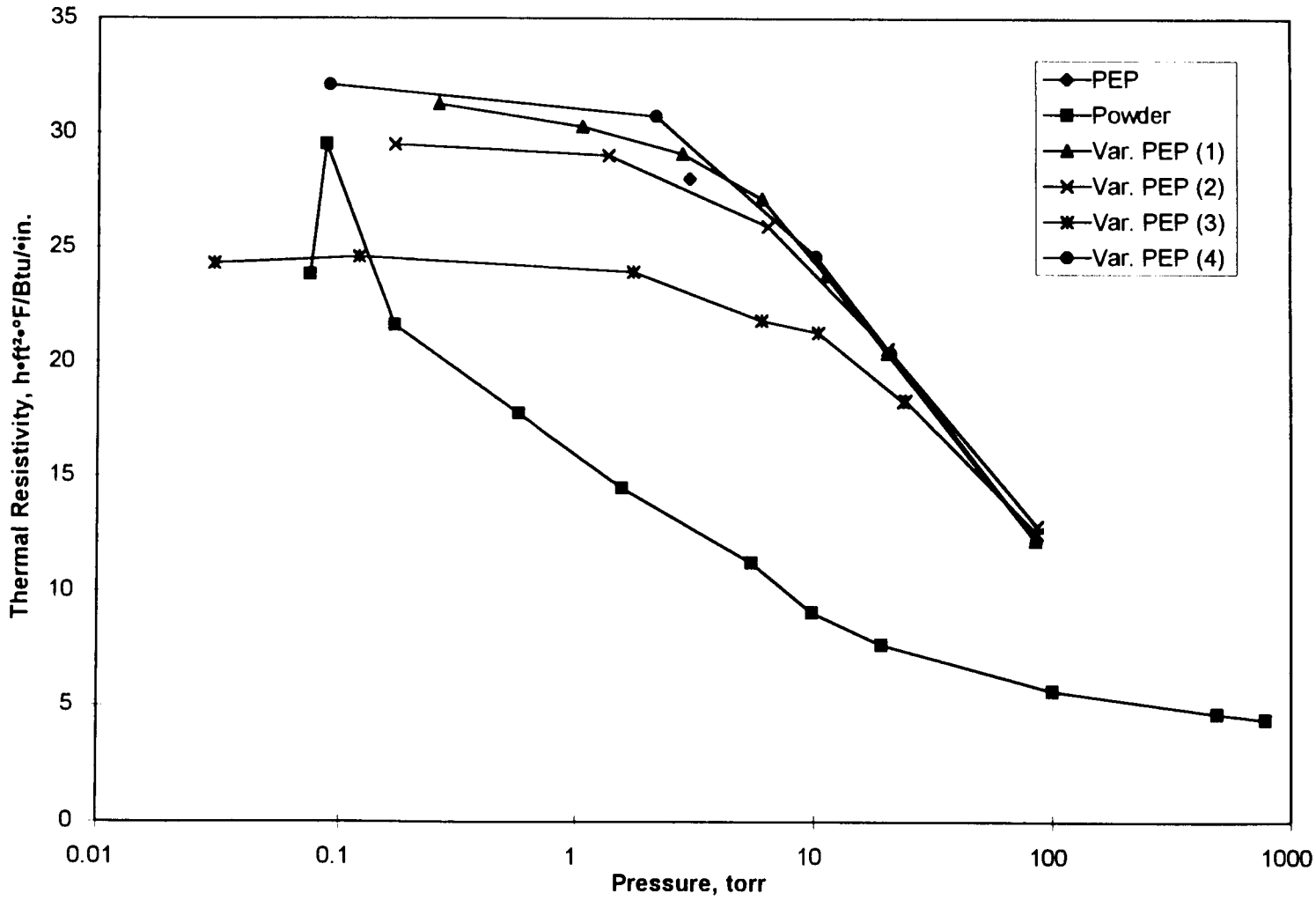

Figure 13. Thermal Resistivity of BXS-363 PEPs and Powder

fourth panels (those made without any extra pressing) had the best performance and were very similar. The resistivities for the second panel were slightly lower. For the third panel, the low pressure resistivities were the lowest of all the panels measured, but the resistivity at higher pressures were less sensitive to pressure than the other panels.

The low pressures results with BXS-363 show that there is an optimum density. As the powder is compacted from its tapped density to densities obtained under atmospheric loading, the low pressure resistivity rises. Upon further compaction, the resistivity decreases. These low pressure trends may be interpreted as being due to an initial decrease in radiation heat transfer during initial stages of compaction, and then an increase in solid conduction upon further compaction.

At intermediate pressures, compaction from the tapped density powder to a panel increases the resistivity by a large amount. This change may be interpreted as a decrease in gaseous conduction heat transfer due to more closely packed particles interfering with the mean free path of the gas molecules. (See section on Heat Transfer Mechanisms later in this report.)

Figures 14 through 17 show comparisons between data obtained on tapped powders and the corresponding variable pressure powder evacuated panel. In each case, the density of the PEP was higher than that of the powder. At low pressures, the powders generally had higher resistivities than the panels, while the reverse was true at higher pressures.

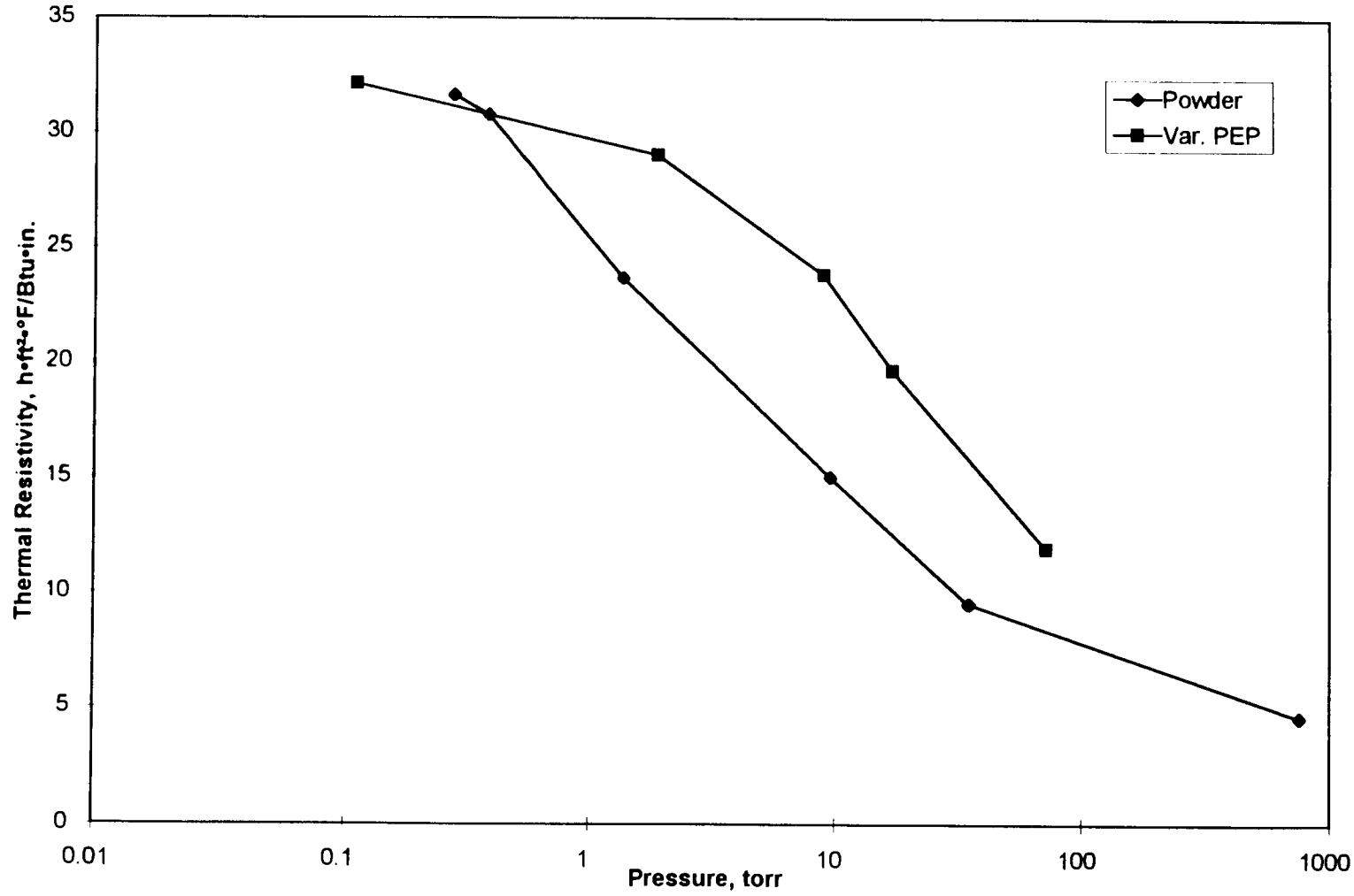

Figure 14. Thermal Resistivity of BXS-424 PEP and Powder

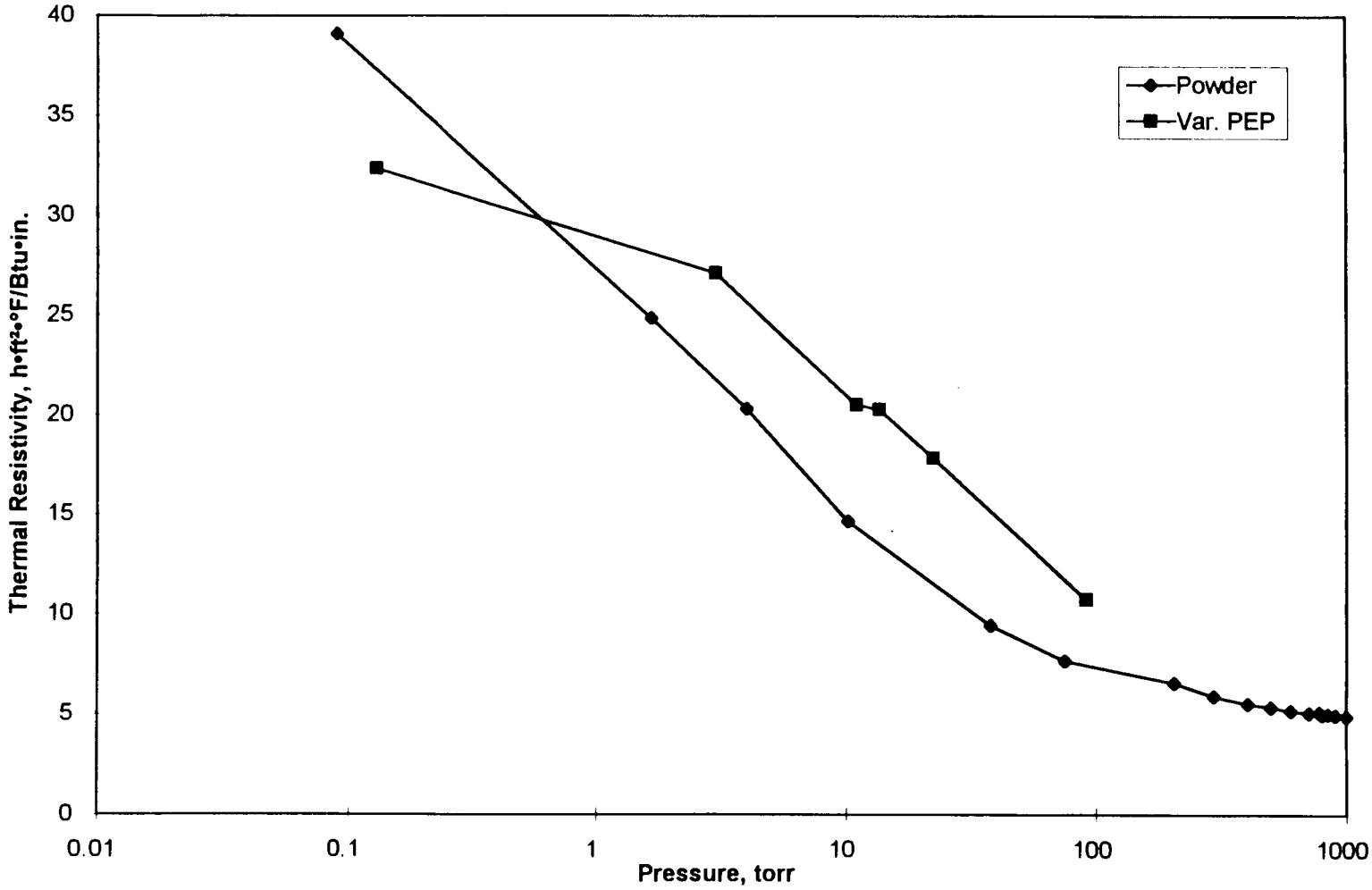

Figure 15. Thermal Resistivity of BXS-426 PEP and Powder

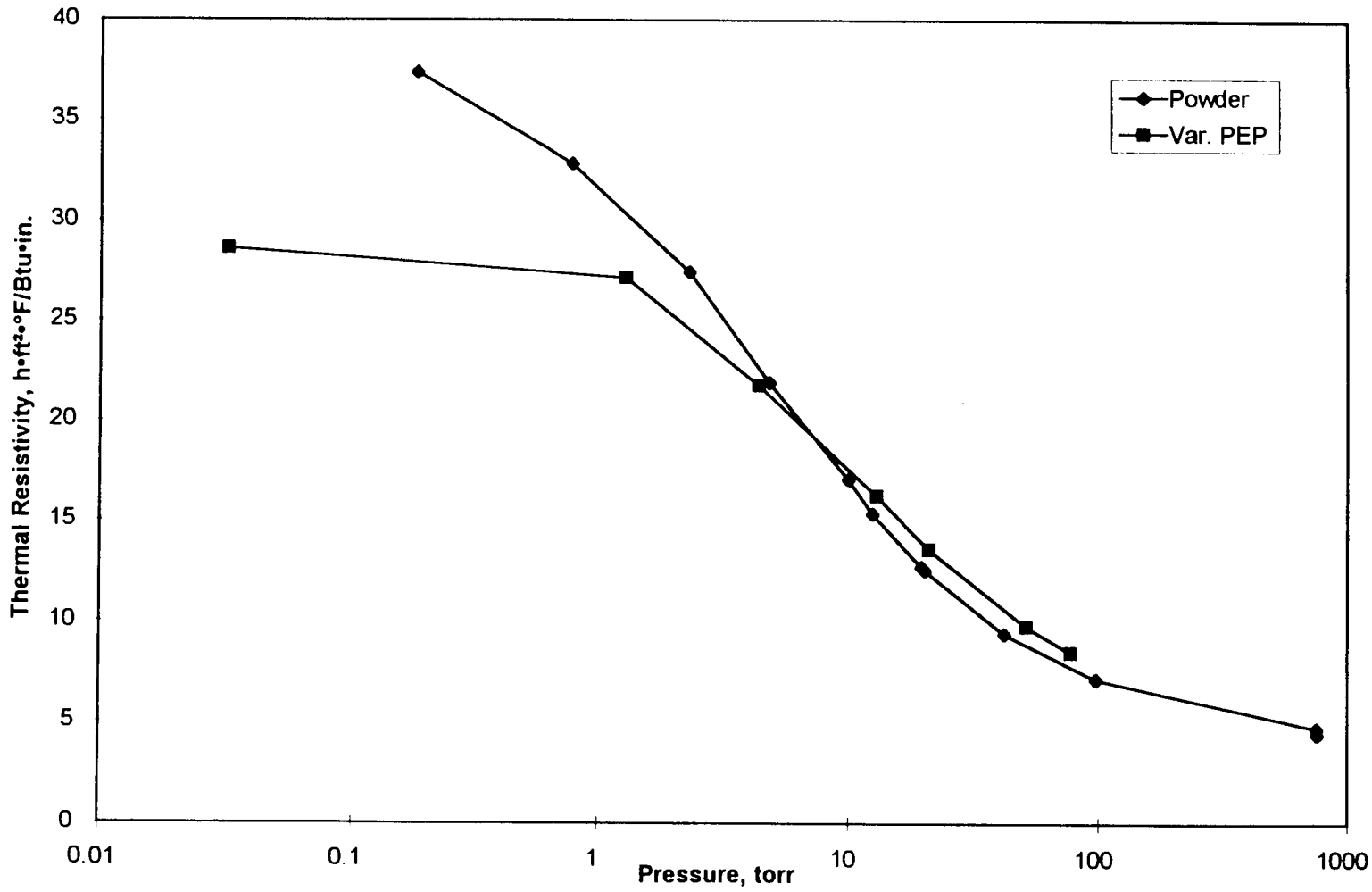

Figure 16. Thermal Resistivity of FK500LS PEP and Powder

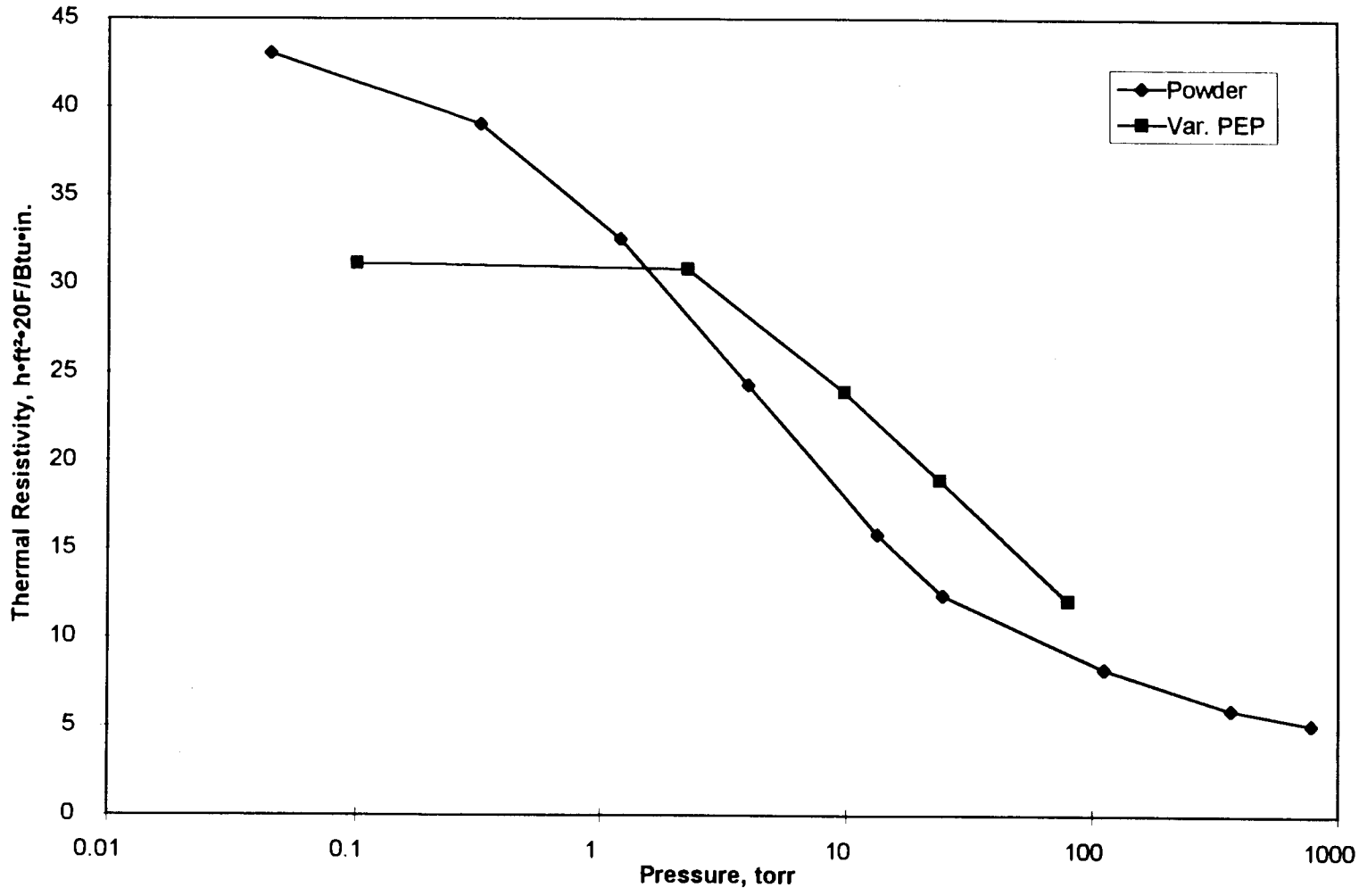

Figure 17. Thermal Resistivity of Sipernat 22 LS PEP and Powder

5. CORRELATION OF HEAT CONDUCTION MECHANISMS WITH MORPHOLOGY

5.1 Heat Conduction Mechanisms

Yarbrough (1) has reviewed the heat flow mechanisms that occur in powders and powder evacuated panel insulation. The three general modes of heat transfer are conduction, convection, and radiation. Convection is the flow of heat by the bulk movement of fluids. Convection is usually considered to be negligible for most types of insulation. For the powders used in PEPs, the particle sizes are so small and the densities are so high that natural convection may be safely ignored.

In powders and PEPs, conduction of heat can occur through both the solid particles and through the interstitial air molecules. In addition, radiation may transport heat across a PEP. The simplest model for heat flow in a powder or PEP is that the thermal conductivity is the sum of the two thermal conductivities due to conduction and radiation:

$$k_{total} = k_{conduction} + k_{radiation} \tag{1}$$

The thermal conductivity component due to conduction is itself a function of the thermal conductivities of the solid and the interstitial gas and of the structure of the powder or PEP.

Normally, the thermal conductivity of a gas is a weak function of the pressure. The effective thermal conductivity of a gas depends on the mean free path of the gas molecules. In bulk gas, the mean free path is determined by the collisions among the gas molecules. In a powder, the mean free path is also determined by collisions of the gas molecules with solid surfaces. Masamune and Smith (2) give the following equation for the effective thermal

conductivity of an interstitial gas in a powder system:

$$k_{gas} = \frac{k^{*}_{gas}}{1 + \dfrac{\left(\dfrac{2 - a}{a}\right)\left(\dfrac{4\gamma}{\gamma + 1}\right)\left(\dfrac{1}{Pr}\right) L_{gas}}{L}} \tag{2}$$

where

$$L_{gas} = \frac{2.331 \times 10^{-20}\ T}{P_{mm}\ \delta^{2}} \tag{3}$$

and

k_{gas} = thermal conductivity of gas at pressure P

k^{*}_{gas} = thermal conductivity of gas at high pressure

a = accommodation coefficient

$\gamma = C_p/C_v$ = specific heat ratio

Pr = Prandtl number

L = spacing between solid surfaces

L_{gas} = mean free path of gas (cm)

T = absolute temperature (K)

δ = collision diameter of gas molecule (cm)

P_{mm} = pressure of gas (torr)

The equation for the effective thermal conductivity of the gas may be simplified by substituting known parameters. In the absence of any specific information, the accommodation coefficient is usually taken to be equal to unity. The mean temperature of the gas in the experiments reported here is 300 K. For nitrogen, the specific heat ratio is 1.4, the Prandtl number is 0.71, and the collision diameter is 3.63 Angstroms (3). With these substitutions, the effective thermal conductivity of the gas is given by:

$$k = \frac{k^*}{1 + \frac{175.4}{P_{mm} L}} \tag{4}$$

where the pressure is in torr and the surface spacing is in microns.

The experimental curves of thermal conductivity versus pressure may be analyzed to obtain estimates of the average surface spacing. For this, it is assumed that the total thermal conductivity is given by:

$$k_{total} = k_o + \frac{\Delta k}{1 + A/P} \tag{5}$$

where k_o is the thermal conductivity of the powder at very low pressures, and $k_o + \Delta k$ is thermal conductivity of the powder at high pressures. With this scheme, k_o can be identified as the sum of the thermal conductivities due to solid conduction and to radiation, while Δk can be identified with the additional thermal conductivity due to air conduction. This simplified picture assumes that the thermal conductivities due to solid and gaseous conduction can simply be added together. More complicated theories are available, but they depend on a better knowledge of the coupling between the two modes of conduction.

Equation 5 can be analyzed by regression techniques to obtain the parameter A, which can then be used to calculate a mean surface spacing from $L = 175.4/A$. Alternatively, the graphs for thermal conductivity versus pressure can be used to read the pressure ($P_{1/2}$) at which $k = k_o + 1/2\ \Delta k$, where Δk is the difference between the highest and lowest measured thermal conductivities. Then another estimate of the mean surface spacing is given by $L = 175.4/P_{1/2}$. Figure 18 illustrates these two methods of estimating the effective surface spacing.

The thermal conductivity due to radiation can be estimated from electromagnetic theory. When the solid particles are small enough, the formulas for Rayleigh scattering and absorption may be used. If the particles are small enough that $\pi D/\lambda << 1$, where D is the mean particle diameter and λ is the wavelength of radiation, then the absorption efficiency, Q_{abs}, is given by

$$Q_{abs} = \frac{24\left(\frac{\pi D}{\lambda}\right) n\ k}{(n^2 - k^2 + 2)^2 + 4n^2k^2} \tag{6}$$

where n is the index of refraction and k is the index of absorption (we use the usual notation for index of absorption, and note that the context should prevent any confusion by using the same symbol for thermal conductivity).(4) The optical constants of silica glass, as functions of wavelength are given in Figure 19.(5) Under the assumed conditions on the relationship between particle size and wavelength, the scattering efficiency is much smaller than the absorption efficiency, and may be ignored. The spectral Rayleigh absorption efficiency is shown in Figure 20.

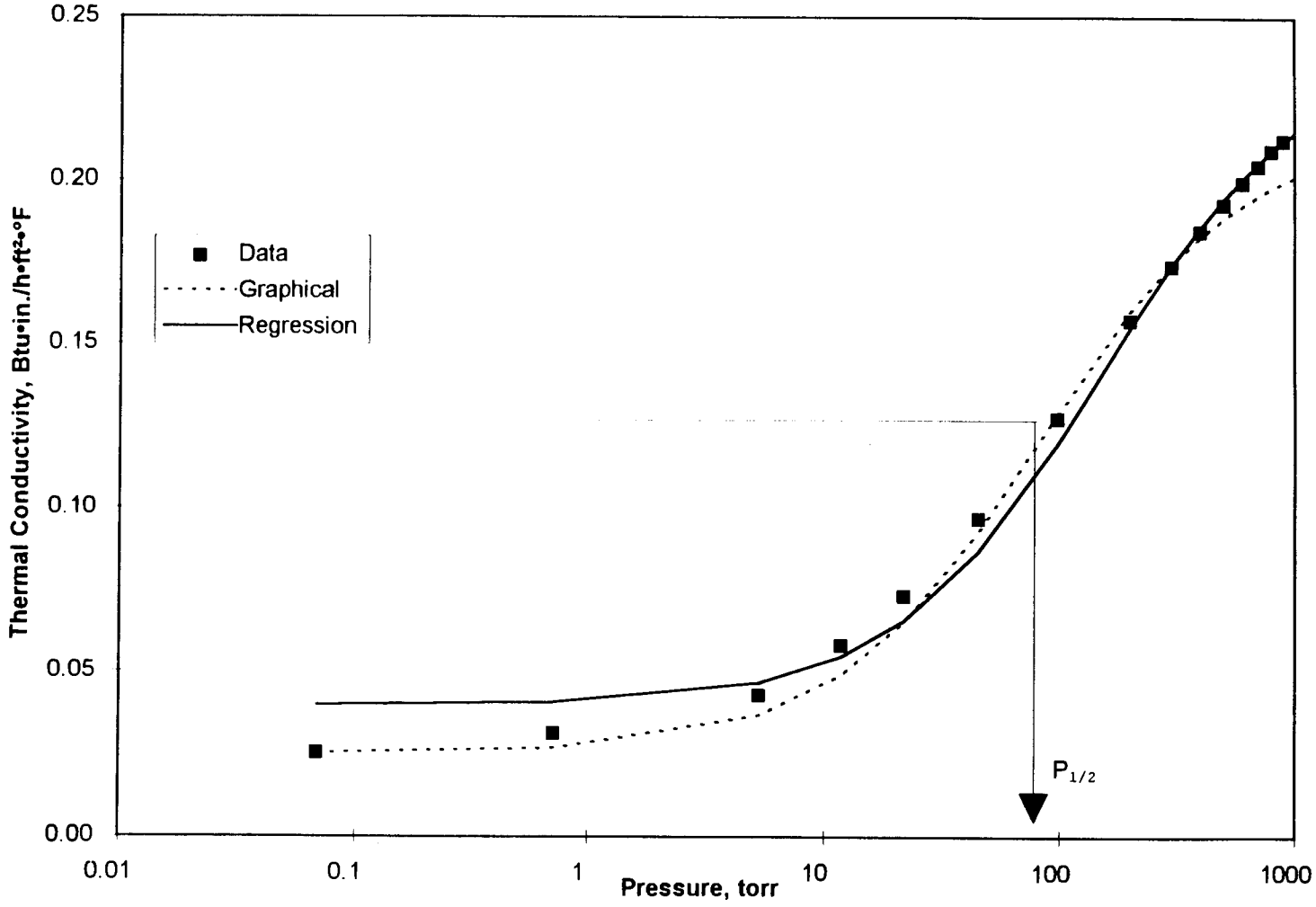

Figure 18. Two Methods to Derive Effective Surface Spacing from Thermal Conductivity versus Pressure Curve (data are for BXS-427 powder)

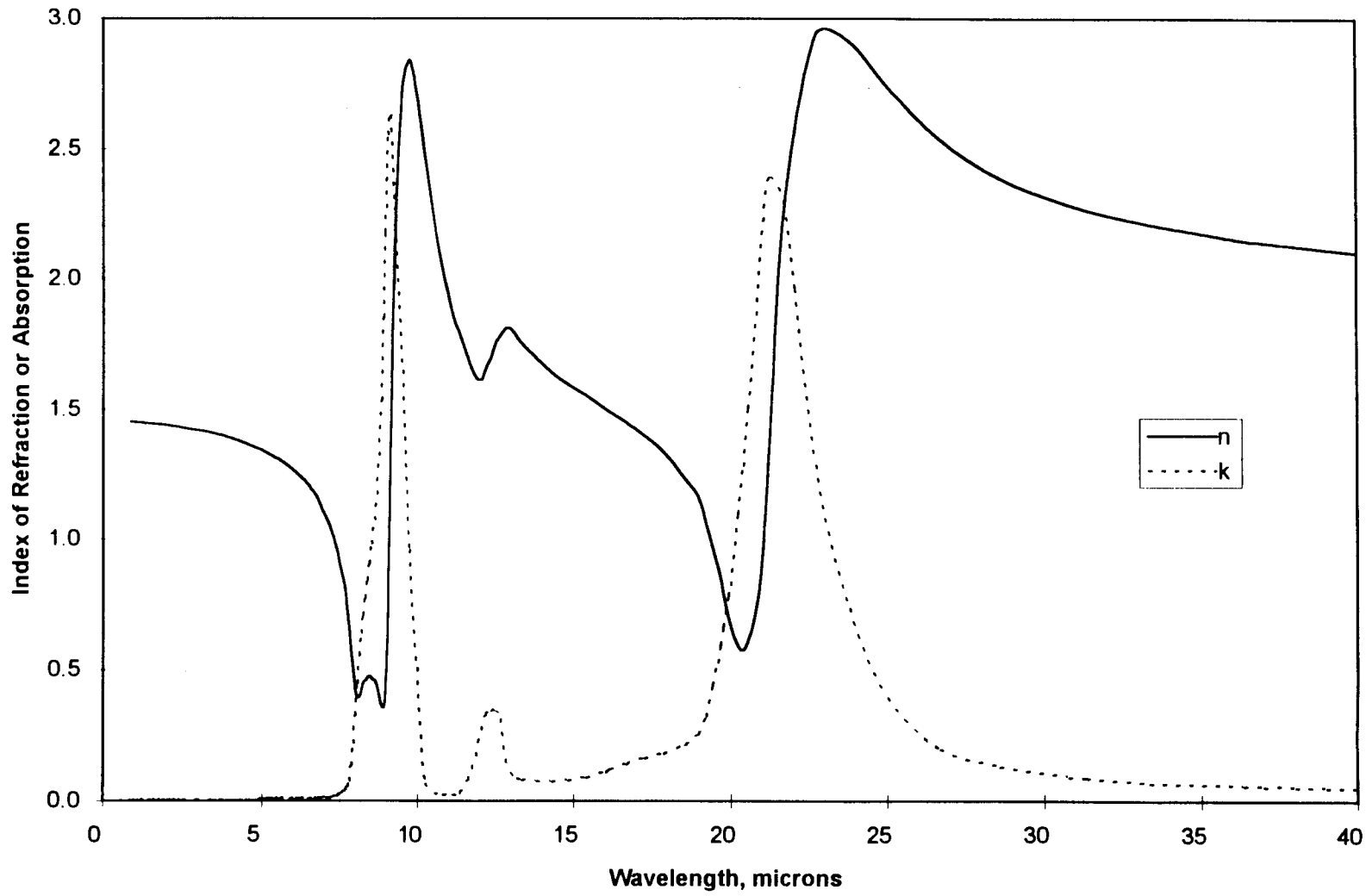

Figure 19. Optical Constants for Silica Glass

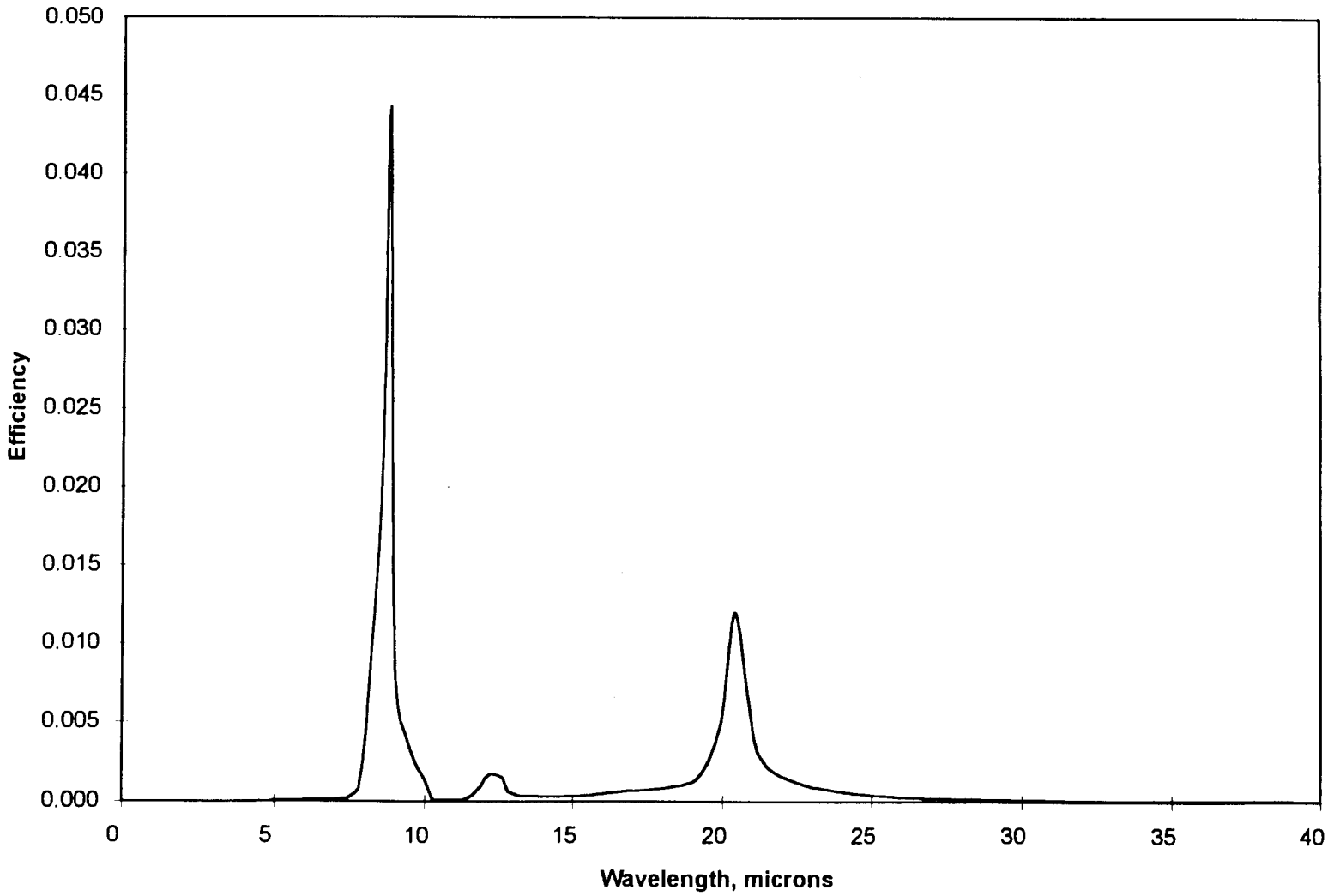

Figure 20. Rayleigh Absorption Efficiency for Silica Glass

Using this absorption efficiency, the absorption coefficient is given by

$$\beta_{abs} = N\, Q_{abs} \frac{\pi}{4} D^2 \tag{7}$$

where N is the number of particles per unit volume. If Equation 6 is substituted into Equation 7, then it will be noted that the absorption coefficient is independent of D and depends only on the volume fraction of solid (or the bulk density). (Note, this conclusion depends on the assumption that $\pi D/\lambda << 1$.)

For the concentric cylinder geometry of the radial heat flow apparatus, Siegel and Howell (6) give the following equation for the radiation heat transfer between the core heater and the outer cylinder wall:

$$Q_{rad} = \int_0^\infty \frac{\pi D_1 L (E_{b\lambda 1} - E_{b\lambda 2})\, d\lambda}{\frac{8}{3} \beta_\lambda D_1 \ln\left(\frac{D_2}{D_1}\right) + \left(\frac{1 - \epsilon_1}{\epsilon_1} + 1/2\right) + \left(\frac{D_1}{D_2}\right)\left(\frac{1 - \epsilon_2}{\epsilon_2} + 1/2\right)} \tag{8}$$

where

D_1 = diameter of inner cylinder

D_2 = diameter of outer cylinder

L = length of cylinder

ϵ_1 = emittance of inner cylinder

ϵ_2 = emittance of outer cylinder

$E_{b\lambda 1}$ = blackbody spectral emissive power of inner cylinder

$E_{b\lambda 2}$ = blackbody spectral emissive power of outer cylinder

β_λ = spectral absorption coefficient, given by Equation 7

λ = wavelength

With this radiation heat flow, a thermal conductivity due to radiation may be calculated from

$$k_{radiation} = \frac{Q_{rad} \ln\left(\frac{D_2}{D_1}\right)}{2\pi L (T_1 - T_2)} \tag{9}$$

where T_1 and T_2 are the temperatures of the inner and outer cylinders.

The normalized integrand of Equation 8-9 with and without a powder with a bulk density of 0.1 g/cm^3 is given in Figure 21. This shows that the presence of the powder greatly reduces the radiation heat transfer that would exist in its absence.

For radiation heat transfer between two parallel plates, the analog to Equations 8 and 9 are

$$Q_{rad} = \int_0^{\infty} \frac{(E_{b\lambda 1} - E_{b\lambda 2})\, d\lambda}{\frac{3}{4}\beta_\lambda L + \frac{1-\epsilon_1}{\epsilon_1} + \frac{1-\epsilon_2}{\epsilon_2} + 1} \tag{10}$$

and

$$k_{radiation} = \frac{Q_{rad}}{(T_1 - T_2)} \tag{11}$$

where L is the separation of the two plates.

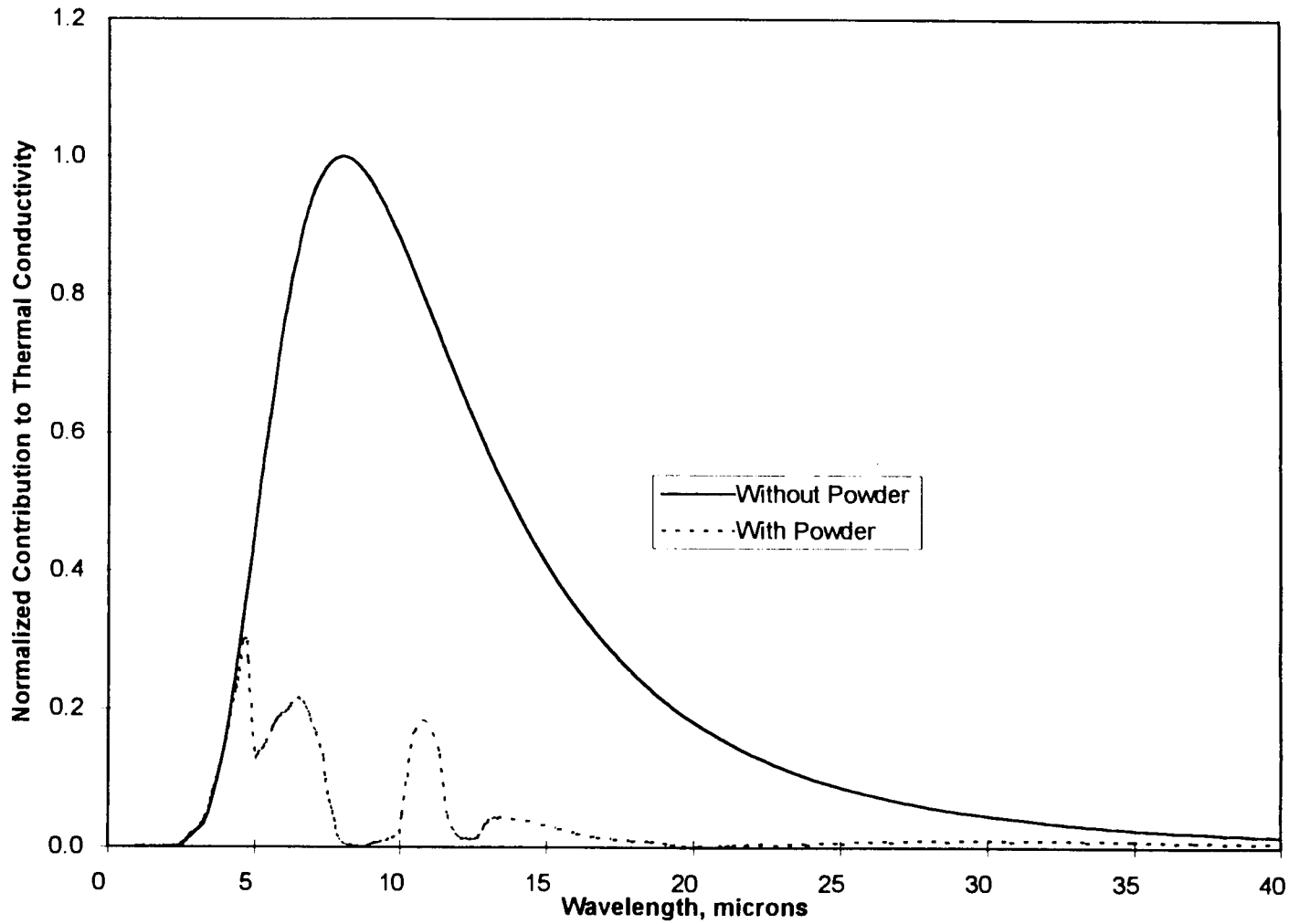

Figure 21. Normalized Spectral Contribution to Thermal Conductivity with and without Powder at 0.1 g/cm^3

5.2 Correlation of Powder Characteristics with Thermal Conductivity

Table 13 gives the results of analyzing the thermal conductivity versus pressure curves for the tapped density specimens to determine the effective surface spacing. The table also give the pressure for which the thermal conductivity is half way between the lowest and highest values. Effective spacings derived by the two different techniques are compared in Figure 22. For this comparison, the data for fly ash were not used since the densities of the fly ash specimens were so much higher than those for the other powders. Also, the data for Y 121-3 and the unmicronized ORNL powder were not plotted because of the incompleteness of the curves of conductivity versus pressure. Figure 22 shows that in general there is reasonable agreement between the two methods of deriving an effective surface spacing. It should be noted that the correlation is highly leveraged by the point for unmicronized Microcel E (the point in the upper right hand corner).

An attempt was made to correlate the effective surface spacing with characteristics of the powder specimens. Coefficients of determination are shown in Table 14. From this table, it is seen that there is very little correlation between the effective spacing and powder characteristics. The best correlation was obtained with the mean particle diameter, as shown in Figure 23. Again, note that this correlation is highly leveraged by the point for unmicronized Microcel E. It is interesting that the effective surface spacing is about two to three times the mean particle size. A better test of this correlation would depend on obtaining thermal data on powders that have a wide range of particle diameters. However, Figure 23 confirms the earlier conclusion that reducing the particle size by micronizing acts to shift the thermal conductivity versus pressure curves to higher pressures, by reducing gaseous conduction at any given pressure.

[redacted]

Table 13. Estimates of Effective Interparticle Spacing for Powders at Tapped Density

Specimen	Graphical $P_{1/2}$, torr	Graphical Spacing, microns	Regression Spacing, microns
FK500LS	68.4	2.56	1.20
Sipernat 22 LS	70.7	2.48	1.26
T-600	44.2	3.97	2.20
BXS-363	21.5	8.14	2.80
BXS-365	36.5	4.84	2.66
BXS-420	34.9	5.02	4.68
BXS-421	37.2	4.71	4.26
BXS-422	45.7	3.84	3.24
BXS-423	61.7	2.84	3.01
BXS-424	59.2	2.96	2.84
BXS-425	63.7	2.75	2.63
BXS-426	49.0	3.58	1.33
BXS-427	82.1	2.14	1.19
BXS-451	43.7	4.01	2.48
BXS-454	43.9	3.99	3.09
Y 121-3	20.6	8.53	0.82
Y 129-2	31.8	5.52	4.85
Y 129-3	49.8	3.52	2.74
Microcel E, Unmicron.	10.7	16.4	11.5
Microcel E, Micronized	46.0	3.82	3.16
Microcel 80/20, Micron.	38.5	4.56	2.84
ORNL, Unmicronized	6.32	27.7	4.51
ORNL, Micronized	69.9	2.51	1.69
Fly Ash, Treated	35.6	4.93	3.36
Fly Ash, Micronized	109.3	1.60	0.827

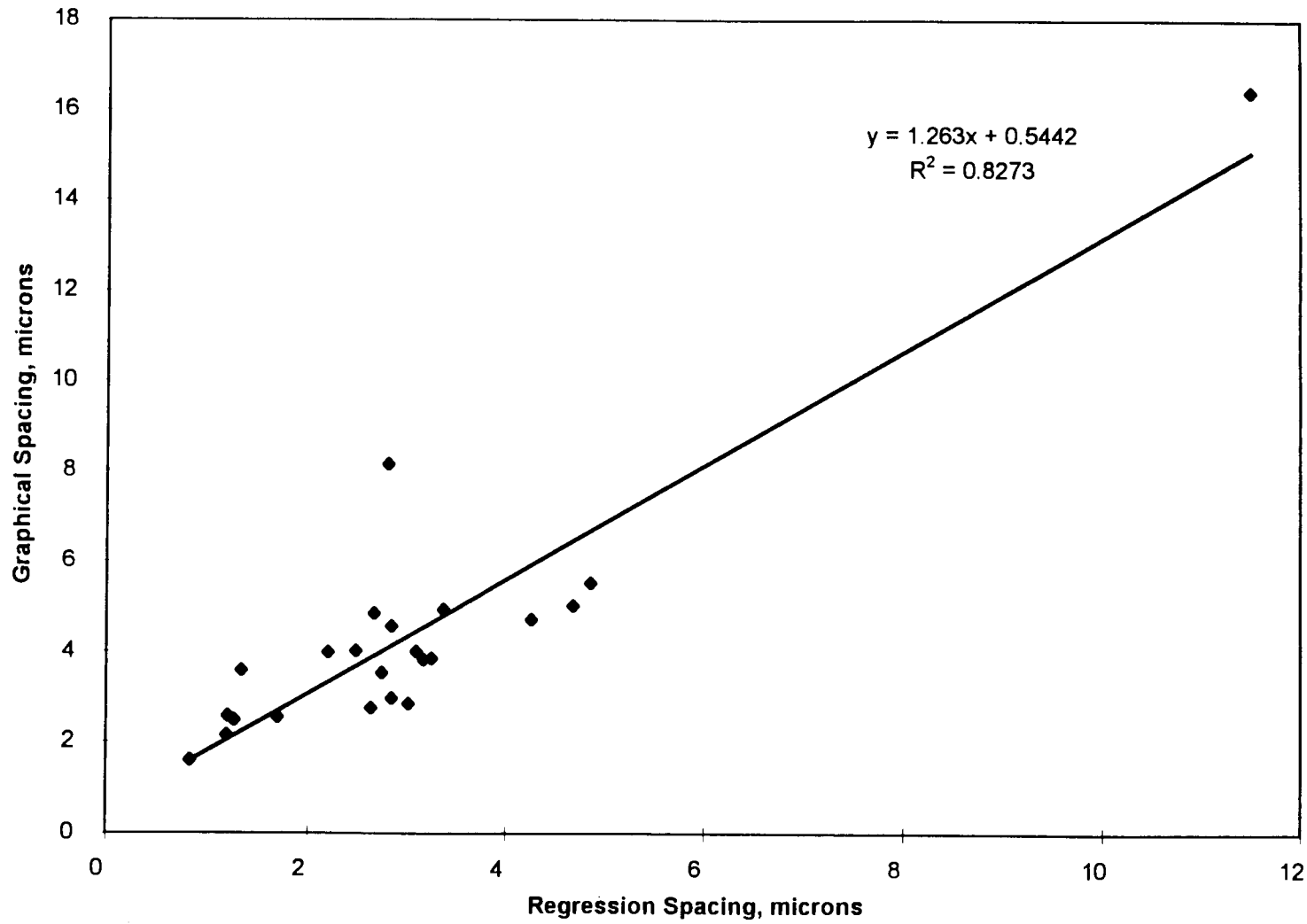

Figure 22. Comparison of Two Ways of Estimating the Effective Surface Spacing

[redacted]

Table 14. Correlations of Graphically Determined Effective Surface Spacing with Specimen Characteristics

Characteristic	r^2
Mean particle diameter (population dist.)	0.69
Thermal specimen density	0.02
Porosity	0.06
Intruded Volume	0.32
Hg Pore Diameter	0.09
BET Surface Area	0.01
Micropore Area	0.13
N_2 Single Point Value	0.04
Micopore Volume	0.03
Average Pore Diameter	0.02

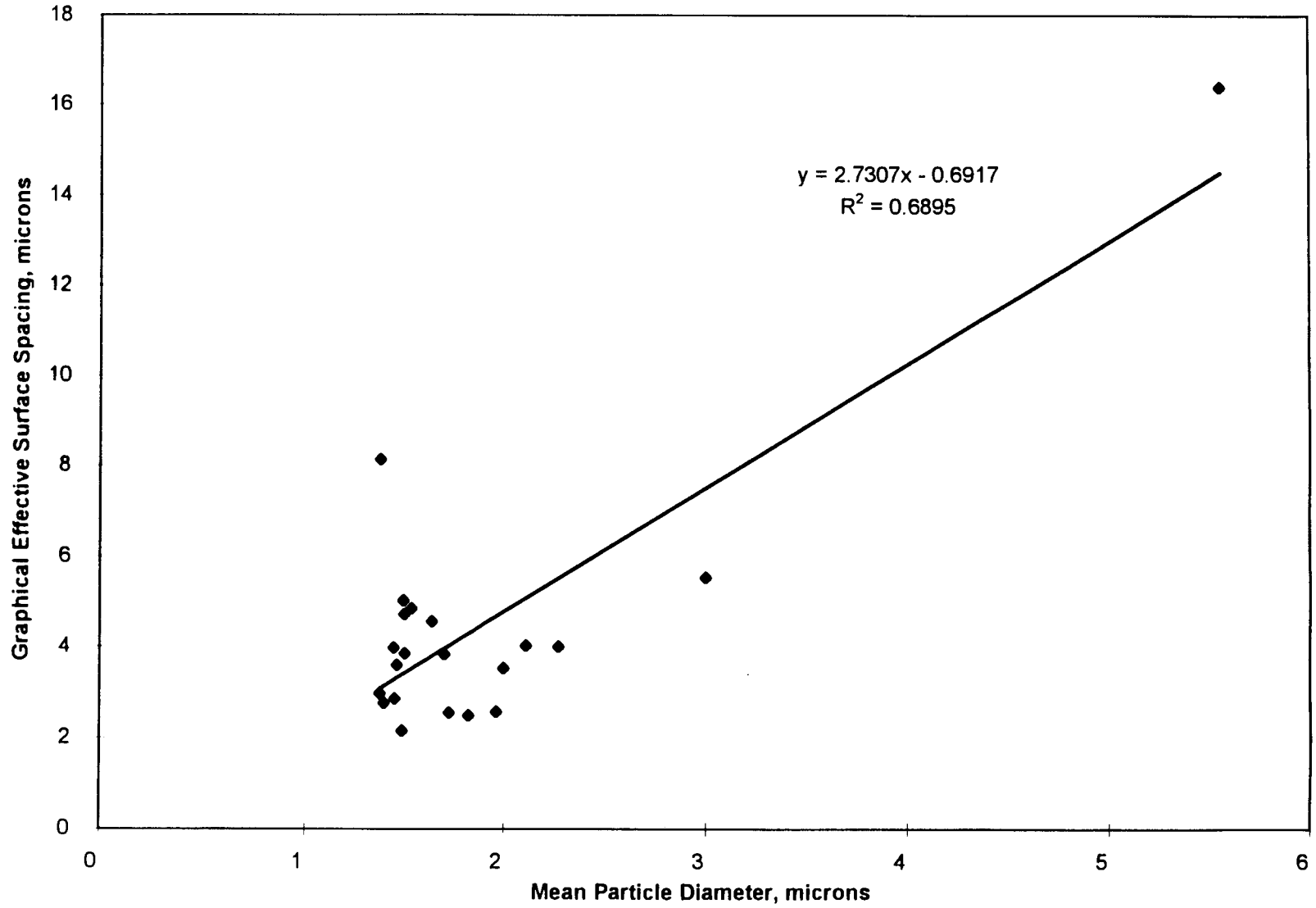

Figure 23. Correlation between Effective Particle Spacing and Particle Diameter

[redacted]

Equations 8 and 9 were used to predict the low pressure thermal conductivity as a function of powder density. Results are shown in Figure 24, where the experimental data are compared with the results of electromagnetic theory for two different assumptions about the infrared emittance of the core heater in the radial heat flow apparatus. The upper curve corresponds to a nearly black core heater, while the lower curve corresponds more closely to the expected emittance of stainless steel at room temperature. This figure shows that the low pressure thermal conductivity data are in reasonable agreement with the results of theory. In general, the trend is for the low pressure thermal conductivity to decrease as the density increases. Assuming that the lower curve is a good representation for the radiation thermal conductivity, the difference between the data points and this curve can be interpreted as the contribution due to solid conduction. It appears that a large fraction, approximately half, of the low pressure thermal conductivity is due to radiation. Further separation of the radiation and solid conduction components could be achieved by measuring the low pressure thermal conductivity over a large range of mean temperatures. The radiation contribution would scale approximately with the third power of the absolute temperature, while the solid conduction would be relatively temperature independent.

The low pressure thermal conductivity of the variable pressure powder evacuated panels is plotted versus density in Figure 25. This shows that the general trend is for the thermal conductivity to increase as the density increases. Comparison of Figures 24 and 25 indicates that the conductivity-density relationship for the panels is beyond the optimum density, indicating that increases in density are leading to increases in solid conduction.

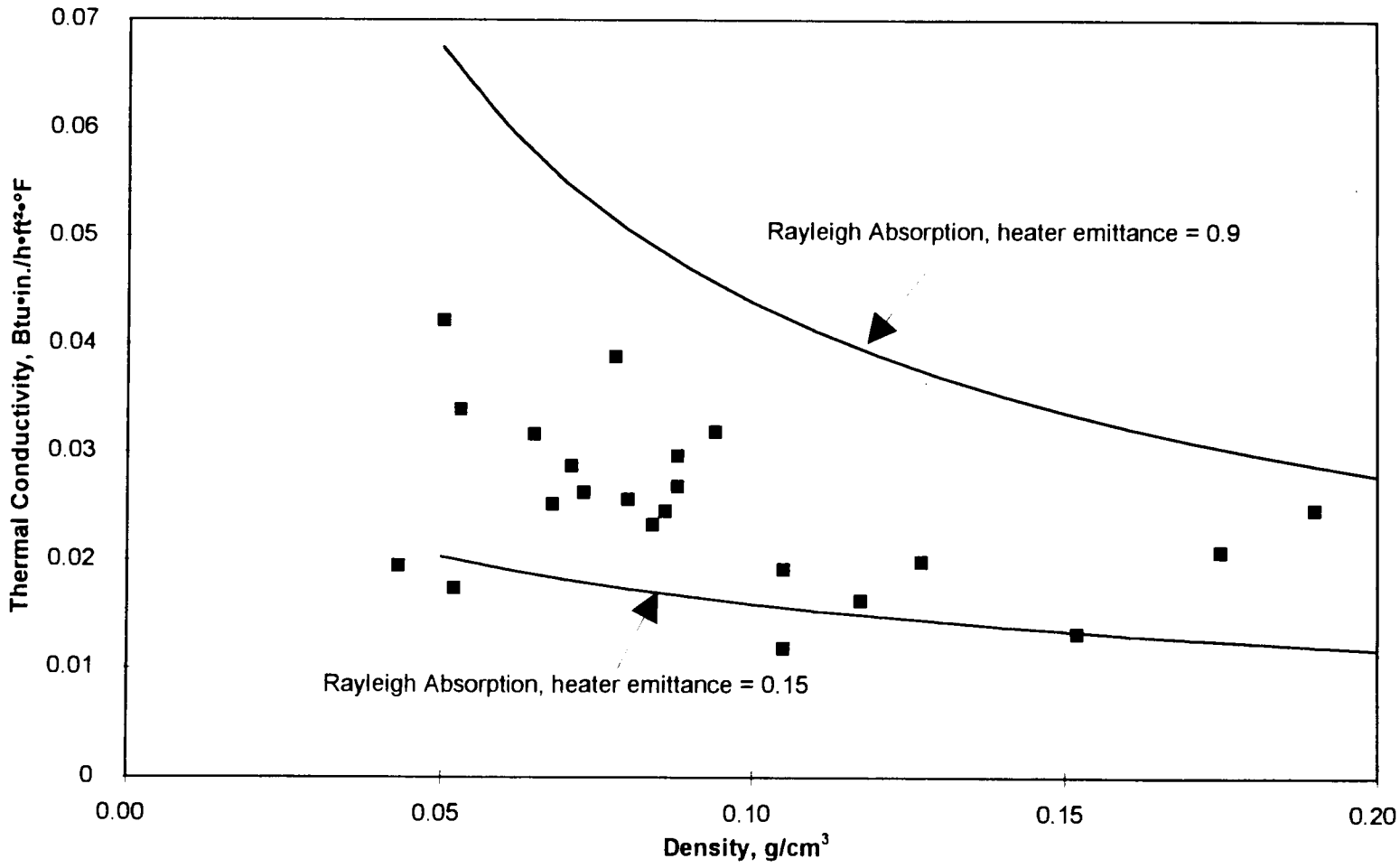

Figure 24. Comparison of Low Pressure Powder Thermal Conductivity with Results of Electromagnetic Theory

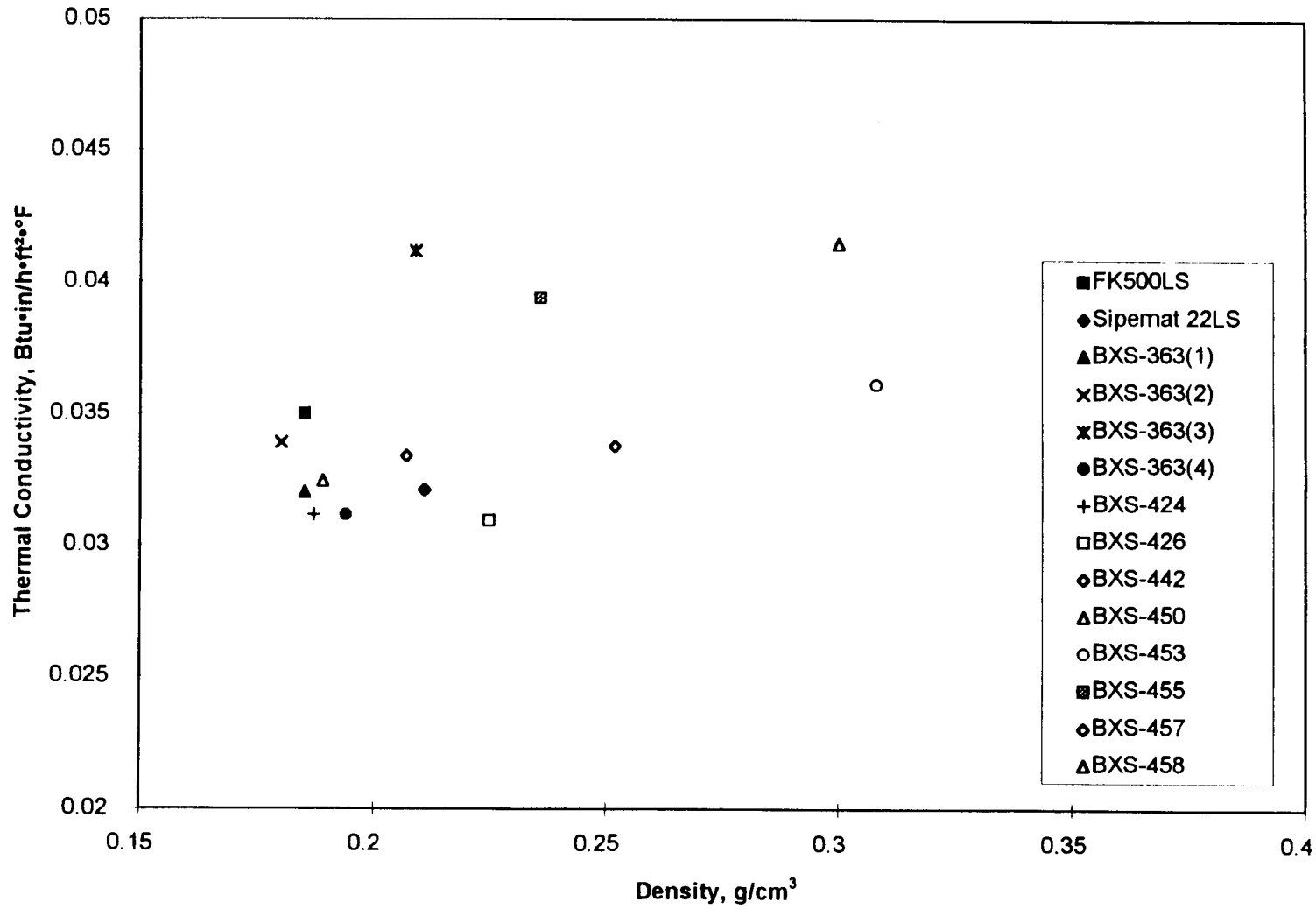

Figure 25. Effect of Density on Thermal Conductivity of Variable Pressure Powder Evacuated Panels

6. COSTS OF POWDERS

The second part of the CRADA objective was to optimize the cost and performance of the PEPs. Due to the timing and costs associated with implementing part one, there were limited resources available for investigating reductions in PEP costs. However, there were two samples which showed some promise: BXS-426 and BXS-457. These samples showed virtually equivalent performance to the other samples, but were manufactured with a 17 to 20 percent reduction in costs. BXS-500 and BXS-501 were synthesized similar to BXS-457 and offer potentially larger cost savings.

7. INVENTIONS

No inventions were made as part of this CRADA.

8. POSSIBLE COMMERCIAL APPLICATIONS

Application of powder evacuated panels to refrigerators and freezers appears to be close to commercialization. Other applications are possible, including walk-in freezers, refrigerated transport vehicles (truck and rail), other home appliances such are water heaters and ranges, commercial ovens, and the envelopes of buildings, especially manufactured housing.

9. CONCLUSIONS AND POSSIBLE FUTURE COLLABORATIONS

The results of the CRADA showed that two factors have a significant role in determining the thermal performance of powders and evacuated panels. First is the particle diameter. As the particle size was reduced by jet-milling, an improvement in the thermal performance was seen.

[redacted]

This was characterized as a lessening in the vacuum requirements to obtain a given level of thermal performance. The second factor was powder or panel density. The results suggested the existence of an optimum density. For powders at tapped density, the trend was for the thermal conductivity to decrease as the powder density increased. For panels (which have higher densities than the tapped powder), the trend was for the thermal conductivity to increase with increasing density. Efforts to correlate thermal performance with other measures of silica morphology were unsuccessful.

It is evident that the only true measure of thermal conductivity can be obtained by measurements on actual panels. Measurements on tapped density powders are not good indicators of the performance in a panel. This appears to be due to the large differences between densities of the panels and the powders from which they are made.

It was demonstrated that the performance of the panels could be maintained while the cost to produce the powders could be reduced by approximately 17 to 20 percent. Special blends of silica with low cost powders and modifications to manufacturing process can be attributed for these potential savings gains.

There are no specific plans for future collaborations. However, it is expected that the ORNL Building Materials Program would be able to perform thermal measurements on especially outstanding candidate powders that PPG may develop in the future.

10. REFERENCES

1. D. W. Yarbrough, "Literature Review: Heat Transfer Through Two-Phase Insulation Systems Consisting of Powders in a Continuous Gas Phase," EPA-600/R-92-203; ORNL/M-2426, Oak Ridge National Laboratory, Oak Ridge, TN, December 1992.

2. S. Masamune and J. M. Smith, "Thermal Conductivity of Beds of Spherical Particles," Ind. and Engr. Chem. - Fundamentals 2 (2), 136-143 (1963).

3. S. Dushman, Scientific Foundations of Vacuum Technique, 2nd Ed., pg. 30-32, John Wiley & Sons, Inc., New York (1962).

4. C F. Bohren and D. R. Huffman, Absorption and Scattering of Light by Small Particles, pp 135-136, John Wiley & Sons, Inc., New York (1983).

5. Handbook of Optical Constants of Solids, pp. 749-763, Academic Press (1985).

6. R. Siegel and J. R. Howell, Thermal Radiation Heat Transfer, 2nd Ed., p. 533, McGraw-Hill, New York (1981).

DISTRIBUTION LIST

1-6. Ken Wilkes, Principal Investigator, Bldg. 4508, MS 6092.

7. Brian B. Bovee, OTT Business Manager, Bldg. 701SCA, MS 8242.

8. Science Technology Partnerships Office, Bldg. 6026E, MS 6396.

9-14. PPG Industries, Inc., Technical Center, 440 College Park Drive, Monroeville, PA 15146

15. Peter Scofield, Department of Energy, EE-421, 5E-098/FORS, 1000 Independence Ave., S.W. Washington, DC 20585

16-17. DOE, Office of Scientific and Technical Information, Office of Information Service, P.O. Box 62, Oak Ridge, TN 37831

18. Office of Patent Counsel, Bldg. FED, MS 8751

19. R. O. Hultgren, Deputy Assistant Manager, Energy Research and Development, DOE-ORO, Oak Ridge, TN 37831-6269

20. Laboratory Records, Bldg. 4500-N, MS 6285

21-25. M&C Records Office, Bldg. 4508, MS 6094